Microchemical Journal 209 (2025) 112676

Contents lists available at ScienceDirect

Microchemical Journal

journal homepage: www.elsevier.com/locate/microc

Gas-sensing properties of In_2O_3-Au sensors as a function of gold particle size and method of their synthesis

M. Ivanovskaya [a], E. Ovodok [a,*], D. Kotsikau [b,c], I. Azarko [b], M. Micusik [d]

[a] Research Institute for Physical and Chemical Problems of the Belarusian State University, Minsk, Belarus
[b] Belarusian State University, Minsk, Belarus
[c] Biomagnetic LLC, Minsk, Belarus
[d] Polymer Institute, Slovak Academy of Sciences, Bratislava, Slovakia

ARTICLE INFO

Keywords:
Colloidal gold
Indium oxide
Thick film gas sensor
Reducing gases

ABSTRACT

Powdered samples of In_2O_3–Au (0,1 wt%) with Au particle size of 1.5 nm and 3.5 nm have been obtained by introducing either colloidal gold particles of a given size or ionic gold into an indium hydroxide sol followed by its drying and annealing at 600 °C. This range of gold particle sizes is of interest for studying adsorption and catalytic properties, since for particles d(Au) ≤ 3.5 nm quantum size effects are observed that determine the properties of gold particles. The structural features of the samples were studied by X-ray diffraction, TEM, ED, IR spectroscopy, EPR and XPS. The sensitivity of In_2O_3–Au thick-film sensors with Au particle sizes of 1.5 and 3.5 nm has been measured to CO, acetone and methane. It has been established that the sensitivity of In_2O_3–Au sensors depends not only on the particle size, but also on the method of introducing gold into the oxide matrix. In_2O_3–Au thick-film sensors with $d_{Au} = 3.5$ nm were found to be more active towards CO and acetone compared to $d_{Au} = 1.5$ nm. The responses of In_2O_3 and In_2O_3–Au sensors to methane at 360 °C are nearly equal and do not depend on either d_{Au} or the method of Au introduction. In contrast, the highest sensitivity at temperatures above 400 °C is demonstrated by In_2O_3–Au layers with $d_{Au} = 1.5$ nm when gold was introduced in ionic form rather than in colloidal. It was found that introducing gold ions leads to the most significant increase in the electrical resistance of the sensors over the entire range of operating temperatures (300–470 °C) and results in a high response to methane. The fixation of gold on the lateral faces of indium oxide crystals causes the emergence of energy barriers, which impede current transfer in the polycrystalline layer of In_2O_3–Au. At the same time, introducing colloidal gold particles does not have such a significant effect on the electrical resistance of the sensors. The obtained results also show that the contact area between the oxide and gold nanoparticles is of great importance, along with the size of Au nanoparticles, when the sensor layer interacts with reducing gases.

1. Introduction

In contrast to bulk state, gold being prepared in nanosized form on the surface of metal oxides is known to exhibit adsorption and catalytic activity [1–3]. A large number of research works are devoted to the study of the catalytic activity in oxidation reactions of fine Au particles on the surface of various oxide supports (Fe_2O_3, NiO, Co_3O_4, ZnO, CeO_2, Al_2O_3, TiO_2, MgO, zeolites), for example [4–14]. Most of the studies on the catalytic activity of nanosized gold were carried out by M. Haruta et al. The properties of most of the studied oxides doped with gold nanoparticles (AuNPs) are summarized in [1]. The high catalytic activity of such materials in the low-temperature oxidation of CO has been demonstrated. It is emphasized that low-temperature heterogeneous oxidation of CO occurs effectively only when the size of AuNPs does not exceed a certain value [3,4,7,10].

However, there is ambiguous data on the optimal sizes of gold particles active in catalysis, since the activity also depends on the nature of the support. It was shown in [6,11,14] that the most active in catalysis are gold particles with sizes of 3 ÷ 3.5 nm. However, a high activity of gold particles with size less than 2 nm was demonstrated in [9]. There are experimental results showing that a high effectiveness of CO oxidation is achieved on single oxides (NiO, Ce_2O_3) modified with Au with average d_{Au} ~ 4.8–6.8 nm, however, the activity depends on the size and morphology of the oxide carrier particles [8].

* Corresponding author.
E-mail address: ovodok@bsu.by (E. Ovodok).

https://doi.org/10.1016/j.microc.2025.112676
Received 25 November 2024; Accepted 3 January 2025
Available online 10 January 2025

According to theoretical concepts, the most significant changes in the properties of AuNPs caused by the quantum size effect are observed at $d_{Au} = 2–3.5$ nm [3,6,12]. Therefore, AuNPs of this size range is expected to be optimal for catalytic applications. Along with the size of the Au particles, the properties of the oxide support can influence the activity of atoms at the Au /oxide interface. Metal oxides might also exhibit their own catalytic effects, especially when prepared in nanosized state [13–15]. The effect of the nature of the carrier is more pronounced in case of semiconducting oxides as compared to insulators [8,15–18]. The Au/oxide contact is more important than the Au particle size for some semiconductor oxides [18]. Therefore, the activity of larger gold grains on semiconductors is higher. The ambiguity of the available data on the sizes of Au particles that are most active in adsorption and catalysis is evidently caused by the fact that the influence of the oxide matrix on the state of gold, as well as the catalytic effect of the oxide are not fully taken into account. Therefore, a comparison of the activity of AuNPs on various oxides supports is important for understanding the adsorption and catalytic processes occurring in Au/oxide materials.

In all known methods of preparation of Au /oxide-support nanocomposites, gold particles with sizes of 1.5–3 nm have a hemispherical shape, which contacts through a flat surface with the oxide matrix along a certain crystallographic orientation [6,10,11,15]. An epitaxial growth of Au particles on oxides is also possible under certain conditions [15]. The perimeter of the Au /oxide-support contact and the oxygen atoms at the interface are active in adsorption and catalytic processes [10,11,18]. The electronic interaction between gold and oxide leads to the stabilization of the adsorption- and catalytically active state of gold and oxygen on the oxide surface. When heated, the interaction between the components can be accompanied with the transfer of electron density, stabilization of the oxidized states of gold – Au^{3+} and Au^{+}, as well as the formation of mixed Au_xMe clusters [7,17]. Advances in understanding the electronic and chemical interactions of the metal/oxide interface are reviewed in [19]. It is stressed that the metal/oxide contact is of greater importance than the size of the metal particles. The important role of oxidized states of gold in the process of catalytic oxidation of CO has been experimentally confirmed in [7]. However, it is not necessary for some Au /metal oxide materials in order to achieve their high activity [6,17].

Most studies deal with the catalytic activity of supported AuNPs in the low-temperature CO oxidation reaction. The mechanism of this reaction was studied using the isotopes ^{16}CO, ^{18}CO and $^{18}O_2$ [20,21]. A four-step mechanism assuming the activation of CO and O_2 at the Au/oxide interface was proposed [21]. The Au/TiO_2 system prepared by various methods has been most fully and widely studied [1,6,10,11,17,20,21]. There is no data on the effect of gold on the catalytic activity in the oxidation reactions of other substances, the mechanism of which may be different from the oxidation of CO. An important role of heterogeneous catalysis and catalytically active additives in determining the sensitivity of sensors based on semiconducting metal oxides is well known [22–28]. Therefore, one can expect a correlation between the changes in catalytic activity and adsorption-gas sensitivity of oxide materials doped with AuNPs. However, there may be differences, since the response of the sensors is determined not only by the processes of adsorption and catalysis, but also by the process of charge transfer in the sensitive layer [22,23,29].

It is worth noting that most studies examined the properties of sensing layers with high gold content (2–4 wt%). One can assume that at this concentration, AuNPs have sizes exceeding those optimal for effective catalysts in CO oxidation processes. A considerable attention to the size of gold particles, their activity and interaction with the carrier oxide is only paid in works devoted to catalysis. In the studies on the sensor properties of "Au/metal oxide", the size of gold particles is not given due attention, although, as is known from the literature on gold nanoclusters, their electronic properties significantly depend on the size [2,3,6]. The size of AuNPs is not taken into account when discussing possible detection mechanisms. The effect of gold on the detection mechanism is mainly considered for SnO_2–Au materials, less often for ZnO–Au [25,28–30]. A favorable effect of gold on the efficiency of SnO_2 sensors to CO was shown in [28] to be typical of both nanosized and micron-sized gold particles, i.e. the effect is associated with Au itself. Nevertheless, the response is significantly enhanced with decreasing the grain size of gold. However, the structural and electrophysical properties of SnO_2 and In_2O_3 differ significantly and, therefore, generalizations are not always applicable.

As has been established in our previous studies, the gas-sensing properties of layers based on SnO_2–Au (0.2 wt%) towards CO, methane, ethanol and acetone depend significantly on the method of introducing gold into the oxide material [31,32]. A difference in sensitivity was revealed when colloidal gold or Au^{III} ions were introduced into SnO_2 at the same size of the resulting AuNPs. The influence of gold on the properties of In_2O_3 sensors and the mechanism of detection of various substances is considered [30,33–35]. The successes and problems of functionalization of the surface of AuNPs metal oxides for use in sensors are analyzed in the review [30]. Among the revised methods of formation of sensitive layers, the introduction of colloidal gold is not considered. The properties of In_2O_3–Au sensors were only studied upon deposition or introduction of Au^{III} in the amount of 0.5 wt% or higher [33,34]. A high threshold sensitivity to CO (0.4 ppm) under pulsed heating is demonstrated, which exceeds the sensitivity of known commercial CO/CH_4 sensors. A difference in their properties under detection of CO and methane was revealed [34]. The mechanism of low-temperature detection of CO on In_2O_3–Au was discussed [35].

There is a study dealing with the deposition of colloidal gold (4 wt%) on the surface of a ceramic layer of CeO_2 sensors [36]. It has been established that in this case the sensitivity to both CO and H_2 increases significantly, while to methane practically does not change, and to ethane and propane it decreases. The size of the gold grains is not specified in the paper, the gold concentration was controlled by the number of drops of Au colloidal solution.

As noted above, the deposition of colloidal solutions of gold or other metals (Pd, Pt, Ag) onto oxides leads to dissimilar results in case of CeO_2 and SnO_2 [36]. One can come to an important conclusion that there are differences in the sensitivity mechanism and properties of the sensors when colloidal gold is deposited on the surface of CeO_2 and SnO_2 oxides. The properties of In_2O_3–Au and SnO_2–Au layers are also expected to differ when using colloidal gold solutions.

Therefore, the influence of both the size of AuNPs and the method of their formation on the gas-sensing properties of sensors based on indium oxide is worth studying. The comparison of the results will reveal the effect of the matrix on the activity of AuNPs and the sensitivity of In_2O_3–Au and SnO_2–Au to certain substances. Indium oxide, with its fluorite-like structure, is similar to cerium oxide. Both oxides are characterized by the non-stoichiometry in the form of oxygen vacancies and ease of change of the charge of the metal over a wide range ($In^{3+} \leftrightarrow In^{2+}$, $Ce^{4+} \leftrightarrow Ce^{3+}$) without structural rearrangements [36–38]. These features distinguish In_2O_3 and CeO_2 oxides from the structure of rutile-type SnO_2. The interaction between AuNPs and the oxide matrix is expected to be stronger in case of In_2O_3 compared to SnO_2, given the chemical properties of these oxides and their structural differences. The peculiarities of interaction at the AuNPs/oxide interface can lead to the occurrence of new electronic states that are active in adsorption and catalysis.

It should be noted, however, that indium oxide is not as interesting for the chemo-resistive sensor market as tin dioxide and some other oxides [25,26]. In recent years, In_2O_3 has been studied for detecting acetone vapors and shows high threshold sensitivity when doped with platinum and gold [39,40]. There are numerous studies on the synthesis of indium oxide in the form of crystallites with different morphologies: morphologies such as sphere nanoparticles, hollow nanofiber, porous hollow spheres, hierarchical nanostructure, nanowire and nanotube have been developed for acetone detection) and the study of their gas sensitivity. The results of these studies are analyzed in reviews [24–26].

Such anisotropic morphology and porous structure of In_2O_3 particles makes it possible to increase the gas permeability of the ceramic layer and make a large surface area available for gas adsorption. The study of hybrid structures, including composites based on a 1D/2D structure in the form of "In_2O_3 nanorods/2D $Ti_3C_2T_x$ layers" has shown that it is possible to reduce the detection temperature of organic substances to room temperature [41,42]. In a review [26] devoted to the analysis of studies of the last five years of doping indium oxide with transition metals, a disappointing conclusion was made that despite the numerous studies, no results were obtained that could be of commercial interest. Undoubtedly, the results of these numerous studies on the development of new methods for the synthesis of indium oxide and its modification with active substances contribute to the understanding of the relationship between the oxide structure, surface condition and functional properties. However, for the commercial attractiveness of the developments, a more significant gain in sensor properties is necessary in order to make the replacement of SnO_2 with In_2O_3 economically viable.

The aim of the research was to establish the effect of AuNPs with sizes less than 5 nm on the sensitivity of sensors based on indium oxide. In order to obtain AuNPs of such sizes, colloidal AuNPs and Au^{III} ions were introduced into an indium hydroxide sol followed by drying and heat treatment.

We did not use the impregnation method in this work, since the advantage of the fixation approach over impregnation was previously shown for In_2O_3–Au composites [34]. The study was carried out on samples with a low gold concentration (0.1 wt%) in order to obtain AuNPs of small sizes and to exclude the enlargement of particles (sticking particles together) during heating and crystallization of In_2O_3. The goal of the paper was not to achieve the highest possible sensitivity of In_2O_3–Au sensors, but to find out how the method of obtaining AuNPs and their size affect the sensitivity to certain substances. The magnitude of the effect of the presence of gold in In_2O_3–Au depends on the density of AuNPs in the system [30].

The sensors have been measured towards CO, acetone and methane. Molecules of these substances have electron-donor (reducing) properties in relation to semiconductor metal oxides. However, the mechanism of their detection may differ under certain conditions. The detection by different mechanisms is most often implemented by regulating the operating temperature of the sensor. There are several points of view on the mechanism of detection of both CO and acetone on metal oxide sensors [43–46]. The distinctions in the structure and properties of materials can lead to the implementation of one or another detection mechanism, which is desirable for achieving preferential sensitivity to one or another substance.

2. Experimental

2.1. Synthesis of materials

Indium oxide was synthesized by sol–gel method described in details in our paper published earlier [47]. This approach makes it possible to obtain nanosized particles of indium oxide that is active in adsorption and catalysis. Indium hydroxide was prepared by the sol–gel method starting from $In(NO_3)_3$ aqueous solution using NH_4OH as a precipitator and nitric acid as a sol stabilizer. The sol was dried in air at room temperature to form indium hydroxide xerogel. A powder of In_2O_3 (sample 1) was obtained by calcination of the xerogel at 600 °C in air.

In order to obtain In_2O_3–Au nanocomposites, two ways of In_2O_3 doping with gold were used in the paper: colloidal solution of gold (samples 2, 3) or water solution of $HAuCl_3$ (sample 4) were introduced into the sol of indium hydroxide. The concentration of Au in the composites was chosen to be 0.1 wt%. The formation of In_2O_3-Au nanocomposite structure proceeds under thermal treatment starting from the colloidal solution of indium hydroxide in the presence either Au colloidal particles or Au ions.

Colloidal solutions of nanosized gold were prepared by the reduction of Au^{III} ions with sodium borohydride in the presence of a stabilizer. The well-known sodium citrate (*Cit*) (sample 3) and the less common 5-(2-mercaptoethyl)-1H-tetrazole (*Tet)* (sample 2) were used to stabilize the sols. The procedure for the synthesis of *Tet* is described elsewhere [48]. *Tet* was previously used to stabilize AuNPs on TiO_2 oxide [49]. The formation of tetrazole-stabilized AuNPs occurs in Au^{III} solutions containing 1,2-bis(2-(1H-tetrazol-5-yl)ethyl)disulfane. At the same time, this substance is reduced with sodium borohydride to form 5-(2-mercaptoethyl) [48]. It has been experimentally established that it is impossible to stabilize colloidal gold particles with a diameter of 2 nm or less using citrate ions. The minimum size of colloidal gold particles in this case is 3.5–5 nm. To stabilize smaller particles, S-containing compounds are required, which form stronger complexes with gold [3].

The average diameter was found for tetrazole-stabilized AuNPs to be 1.8 ± 0.2 nm, and 3.5 ± 0.5 nm in case of citrate stabilizer [31]. The colloidal solution of indium hydroxide containing Au nanoparticles was dried in air. The resulting xerogel was heated at 600 °C. Considering the low concentration, the growth of gold particles was not expected under heating due to both the stabilizer and the hydroxide/oxide matrix. When Au^{III} ions are added into a colloidal solution of indium hydroxide, gold ions incorporate into indium oxide structure followed by the transformation into Au^0 state upon heating [47].

The denotations of the prepared samples together with a brief indication of the procedure for their synthesis are given in Table 1.

2.2. Structural characterization

The structure of the samples was studied by electron and *X*-ray diffraction (ED and XRD), transmission electron microscopy (TEM), infrared spectroscopy (IR), electron paramagnetic resonance (EPR) and X-ray photoelectron spectroscopy (XPS).

X-ray diffraction patterns of the samples were recorded on a diffractometer PANalytical X"Pert PRO MRD with CuK_α-radiation. The X-ray diffraction measurements (XRD) was carried out using a Philips X-ray PANalytical Empyrean diffractometer with CuK_α-radiation. The grain size was estimated using a LEO-906E transmission electron microscope. IR spectra were recorded on an AVATAR FTIR-330 spectrometer (Thermo Nicolet) supplied with Smart Diffuse Reflectance accessary within the range of 400–4000 cm^{-1}. EPR spectra were acquired on a VARIAN E 112 spectrometer at 9.35 GHz (*X*-band) and on an ELEXSYS-II E500 CW-EPR (BRUKER) spectrometer (*X*-band) at 77 and 298 K. The *g*-factor values were determined relative to the hyperfine structure (HFS) lines of Mn^{2+}/MgO. X-ray photoelectron spectroscopy (XPS) was carried out by using a Kratos DLD Ultra Spectrometer with an Al*K*α X-ray source (monochromator) operated at 225 W. For the survey spectra a pass-energy (PE) of 160 eV was used while for the region scans PE was 40 eV. Spectra were calibrated to 530.1 eV binding energy (BE) of O1s signal and to 284.8 eV BE of C1s signal. For all samples charge neutralization was necessary. Data evaluation was carried out with CasaXPS software version 2.3.17.

Table 1
Samples of gas-sensing materials based on indium oxide and conditions of their synthesis.

№	Sample	Additive	*T*, °C	Synthesis conditions
1	In_2O_3		600	Sol-gel, $In(OH)_3$, HNO_3 stabilizer
2	In_2O_3–Au, *Tet*	0,1 wt% of Au	600	Sol-gel, $In(OH)_3$, HNO_3 stabilizer, colloidal Au, d_{Au} 2 nm stabilized with tetrazole (*Tet*)
3	In_2O_3–Au, *Cit*	0,1 wt% of Au	600	Sol-gel, $In(OH)_3$, HNO_3 stabilizer, colloidal Au, d_{Au} 3.5 nm stabilized with sodium citrate (*Cit*)
4	In_2O_3–Au^{III}	0,1 wt% of Au	600	Sol-gel, $In(OH)_3$, HNO_3 stabilizer, $HAuCl_4$ solution

2.3. Fabrication of sensors and measuring their parameters

To produce the sensing elements of sensors, the corresponding powders were carefully dispersed in alcohol to form a paste followed by thick film layers formed on sensor microhotplates using this paste. Standard microhotplate made of aluminum oxide substrates with a platinum heater and platinum measuring electrodes were used [31]. The sensing layer thickness was deposited to be 150–175 μm. Two series of five sensors were made from each material. The appearance of the sensor, the sensitive element, microhotplate scheme and the SEM image of the surface of In_2O_3 sensing layer are shown in Fig. 1. The sensing elements were mounted in standard housings. The resistance of the sensors was measured both in air (R_0) and in gas-air mixtures (R_g) under static voltage conditions. The dependence of the sensor characteristics on the operating temperature was evaluated by varying the applied voltage [31]. The sensor responses G were calculated as the ratio of electrical resistance in air and in a gas-air mixture ($G = R_0/R_g$). The compositions of the gas mixtures and relative humidity (RH) were as follows: 100 ppm CO ($RH = 30$ %), 10 ppm acetone ($RH = 98$ %), 0.5 vol % CH_4 ($RH = 30$ %). Standard gas mixtures of air – CO and air – CH_4 intended for calibration of commercial sensors were used. A mixture of air – acetone vapor with high humidity was created to simulate human exhaled air [50].

3. Results and discussion

3.1. Structural characterization of the samples

X-ray diffraction. XRD patterns of indium oxide heated at different temperatures are given in Fig. 2. A xerogel obtained by drying the indium hydroxide sol at 50 °C appears to be a mixture of poorly crystallized phases of $In(OH)_3$ and InOOH. Heating the powder at 200 °C causes the occurrence of pronounced reflexes assigned to C–In_2O_3 with cubic symmetry. Successful annealing at 300, 400 and 500 °C leads to the emerging of rhombohedral indium oxide (R–In_2O_3) as seen in Fig. 2. The rhombohedral phase is thermodynamically unstable at room temperature. However, it is being stabilized in the powder due to a high concentration of structural defects arisen in the run of intense dehydration of indium hydroxide, which is typical of sol–gel method [51].

Further structural rearrangement of R–In_2O_3, along with the thermal removal of NO_x and OH groups, contributes to the formation of oxygen vacancies in the crystal lattice of C–In_2O_3. Calcination of the powder at 600 °C results in disappearing the R–In_2O_3 oxide reflexes (Fig. 2, curve 4). However, the fragments of R–In_2O_3 phase might remain in the sample as shown by ED method.

The X-ray diffraction patterns of In_2O_3–Au samples are similar to those of individual In_2O_3 (Fig. 2b). Increased intensities of the R–In_2O_3 phase reflexes is observed. The occurrence of gold is not detected due to its low content and nano-sized state.

Transmission electron microscopy and electron diffraction. TEM images of samples 1–4 are presented in Fig. 3. The grain size of both indium oxide and gold particles determined by TEM and other methods is given in Table 2. Indium oxide particles have the same morphology in all samples, differing slightly in size. The average diameter of indium oxide decreases in the presence of gold. We were unable to visually detect AuNPs in polycrystalline indium oxide samples due to small size of gold grains. Due to the strong interaction with indium oxide, they can be partially embedded in the matrix or attached to the lateral unfinished faces of indium oxide. Partial immersion of AuNPs in the SnO_2 layer was observed earlier [52]. During the joint formation of Au and In_2O_3, this process is even more probable in C-In_2O_3 with structural oxygen vacancies in the crystal lattice rather than in SnO_2 with a rutile structure. Attachment to the lateral faces and crystal growth steps was observed in the TiO_2–Au system [20]. It was found possible to "tear off" some colloidal gold particles from indium oxide in In_2O_3–Au,*Tet* sample by ultrasonic treatment in methanol. The results obtained confirm that the AuNPs in In_2O_3–Au,*Tet* retain the size that was in the initial colloidal solution. In case of In_2O_3–Au,*Cit* it was not possible to tear off AuNPs, which may indicate a stronger fixation of AuNPs in the In_2O_3 matrix. This gives grounds to assume that in this sample there is also no enlargement of the primary AuNPs due to the stabilizing effect of both citrate shell and In_2O_3. The stabilization of AuNPs particles in In_2O_3 is confirmed by the obtained results discussed below.

The visualization of AuNPs in the In_2O_3–Au^{III} sample became possible after partial dissolution of indium oxide. Thus, after etching the surfaces of In_2O_3–Au^{III} sample in HNO_3 solution, AuNPs with $d_{Au} \sim 1.5$ nm are observed (Fig. 3d). There are also very small particles ($d_{Au} \sim 1$ nm), as well as aggregates of irregularly shaped particles with $d =$ 3.8–4.7 nm. The aggregation of AuNPs occurs after removal indium oxide in which they were anchored. An increase in AuNPs size was observed with increasing etching duration and reaching the completeness of In_2O_3 dissolution. The chosen method of formation of In_2O_3–Au^{III} from $In(OH)_3$–Au^{III} sol, as well as the fluorite-like crystal lattice of C–In_2O_3 with the presence of structural oxygen vacancies, favor the inclusion of AuNPs into the oxide lattice [47].

Electron diffraction did not reveal the presence of gold in In_2O_3–Au^{III} sample, even with an increased gold content of up to 0.2 wt%. The diffraction reflections were observed from the cluster of indium oxide particles in In_2O_3–Au^{III} sample, which the parameters are given in Table 3. Very low-intensity ring diffraction with $d = 2.35$ Å does not allow confirming the presence of gold, since it can also refer to indium oxides: C-In_2O_3 and R-In_2O_3. No gold reflections were detected in the diffraction pattern from individual indium oxide crystals. Point diffraction from individual planes of indium oxide crystal lattice is observed, as shown in Fig. 3e. One of the point reflections (113) in the image can be attributed to R-In_2O_3. The state of gold in In_2O_3–Au^{III} sample can only be predetermined tentatively. The fact that gold particles appear after partial dissolution of indium oxide may indicate encapsulation of AuNPs in the indium oxide matrix. The absence of electron diffraction from Au may have various causes: a flat, very thin particle shape with the (111) plane orientation perpendicular to the electron flow, gold atoms pinned to incomplete side faces, ledges and structural vacancies in indium oxide crystal lattice; formation of particles with an icosahedral rather than cubic structure. All these features of the geometry and arrangement of gold atoms are possible at a particle size of about 2 nm or less. They were previously observed in Au–TiO_2

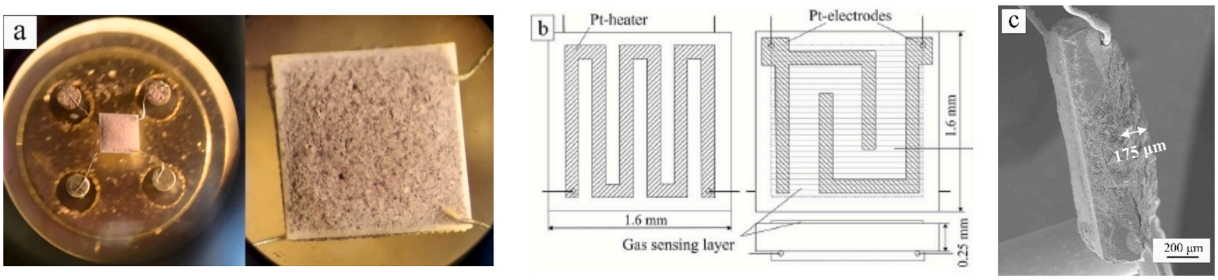

Fig. 1. Photograps of the sensor and sensing element (*a*), and scheme of the microhotplate (*b*), SEM image of the microplatform with the sensing layer (*c*).

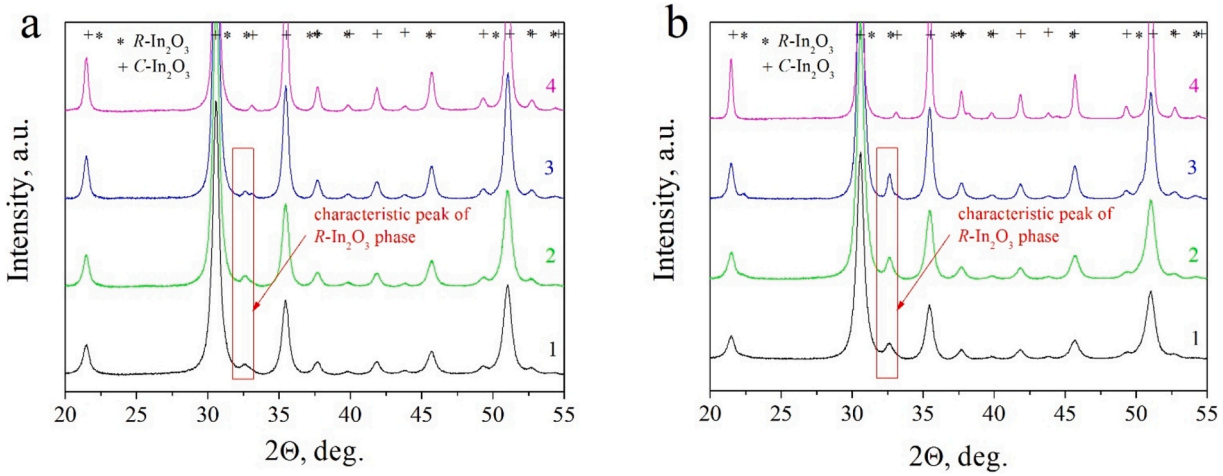

Fig. 2. XRD patterns of In_2O_3 (a) and In_2O_3–Au^{III} (b) samples heated at 300 °C (1), 400 °C (2), 500 °C (3), 600 °C (4).

[16,20]. As shown experimentally, gold was pinned to the edges and ledges of indium oxide grains and other oxides [22].

In a colloidal solution, Au^0 is formed by chemical reduction of Au^{III} in the presence of a stabilizing additive, which ensures the retaining of the highly dispersed state of AuNPs. After thermal degradation of the stabilizing shell, AuNPs are already surrounded by the In_2O_3 matrix. In In_2O_3–Au^{III} sample, the ionic state of Au^{III} changes to Au^0 upon heating to 300–400 °C, although the presence of the oxide matrix can inhibit this process. In this case, the oxide matrix limits the growth of gold particles and prevents their aggregation. The size of gold particles and the nature of their fixation can be evaluated by some indirect indications. Thus, the metallic state of gold and its high dispersion in In_2O_3–Au^{III} are confirmed by studying the plasmon resonance (PR) phenomenon in the 520–540 nm region of optical spectra. Due to the quantum-size effect, a plasmon resonance band appears in the optical spectra of small particles of gold and other metals [3,53]. As found experimentally, the size of gold particles affects not the position of the PR line in the spectrum, but its intensity and width. According to the data reported in [3,53], the PR peak is not recorded at gold particle size of 1.5 nm. An increase in the particle size above 2 nm leads to the emergence of a very weak and wide PR band. In [3], it is shown how the intensity of the PR peak increases without changing the position of the maximum in the case of colloidal gold particles with sizes of 1.5 nm (no PR), 3.4 nm, 5.4 nm, 6.8 nm and 8.7 nm. The particles were stabilized with dodecanethiol. Our studies of plasmon resonance in In_2O_3–Au^{III} thin films with different gold content and heating temperature shown that the size of gold particles at a concentration of 0.1 wt% and a heating temperature of 600 °C does not exceed 2 nm since the PR is not registered. However, the PR band emerges after heating the sample at 800 °C, when the gold particles become larger.

It follows from the presented results that the introduced colloidal gold retains high degree of dispersion under heating to 600 °C and in the run of joint formation of In_2O_3–Au nanocomposites. This temperature is insufficient for more significant changes in the crystalline structure of indium oxide, which occur at 800 °C and cause particle enlargement. As will be shown by the EPR method below, nitrogen-containing fragments of the sol stabilizer will remain in indium oxide after 600 °C thus preventing the ordering of the crystal lattice and the enlargement of *C*–In_2O_3.

Infrared spectroscopy. The IR spectra of the samples are shown in Fig. 4. The results of their analysis are summarized in Table 4.

Gold concentration in the samples is quite low. Hence, any pronounced changes in the spectra related to In–O and In–O–H vibrations were not expected. But still, there are some changes in the frequencies of both characteristic vibrations of In–O and adsorbed/surface groups, which may indicate the effect of gold on the energy of bonds in indium oxide. The shape of the spectra in the region of characteristic vibrations of In–O bonds is the same for all samples and it is typical of indium oxide. The wavenumbers of In–O vibrations are close to both experimental and theoretically calculated values. However, one can note a slight change in the frequencies of certain vibrations, including those related to In–O vibrations.

The following distinctions can be found in the IR spectra of the samples:

1) A decrease in the vibration frequency of ν(In–O) from 415 to 403 cm^{-1} in the spectrum of In_2O_3–Au,*Tet*, while remaining unchanged in the spectra of In_2O_3–Au,*Cit* and In_2O_3–Au^{III}.
2) An increase in the frequency of ν(In–O) from 533 to 537 to 542 cm^{-1} in the spectrum of In_2O_3–Au,*Tet*.
3) A slight increase in ν(In–O) up to 568 cm^{-1} in In_2O_3–Au,*Tet* and a decrease down to 560 cm^{-1} in In_2O_3–Au,*Cit* in comparison to 565 cm^{-1} in In_2O_3.
4) A slight increase in ν(In–O) up to 600 cm^{-1} in In_2O_3–Au^{III} as compared to 595 cm^{-1} in In_2O_3, In_2O_3–Au,*Tet* and In_2O_3–Au,*Cit*.
5) The intensity of ν_3(In–O–H) band at 1118 cm^{-1} is higher in case of In_2O_3 and In_2O_3–Au,*Tet* as compared to In_2O_3–Au,*Cit*; In_2O_3–Au^{III} samples.
6) The intensity of bands at 950 and 1115 cm^{-1} is higher in the spectrum of In_2O_3–Au,*Tet* as compared to pure In_2O_3.
7) A decreased difference between the frequencies of symmetric and asymmetric vibrations of bidentately adsorbed carbonate groups. The following bands have been considered: 1289 cm^{-1} – $\nu_1(CO_3H)$; 1337, 1358 cm^{-1} – $\nu_1(CO_3)$ in CO_3^-; 1419, 1453 cm^{-1} – $\nu_1(CO_3)$, $\nu_4(CO_3)$ in CO_3^{2-}; 1514, 1558 cm^{-1} – $\nu_4(CO_3H)$ in CO_2^- [47]. One can conclude that carbonate groups are adsorbed on the surface of In_2O_3–Au,*Cit* and In_2O_3–Au^{III} samples, while carboxylates (–OCO–) in complex with OH groups are typically adsorbed on In_2O_3 and In_2O_3–Au,*Tet*. The XPS data supports the assignment of the mentioned vibrations to –OCO– groups rather than to NO_x molecules.

The changes in the spectrum of In_2O_3–Au,*Tet* within the region of ν_3(In–OH) vibrations might be caused by the contribution of vibrations related to sulfate groups adsorbed on In_2O_3 surface, which are formed during the decomposition of tetrazole-stabilized AuNPs [49]. Therefore, the observed increase in line intensity in this region of the spectrum is a consequence of the superposition of In–OH and S–O vibrations. The typical bands attributed to sulfate groups are as follows: ν_1 at 948 and 1080, ν_3 at 1105 cm^{-1} [31,54]. Individual hydroxyl groups are retained in both In_2O_3 and In_2O_3–Au,*Tet* samples after their heating at 600 °C.

The results of IR spectroscopy show the similarity of the spectra of

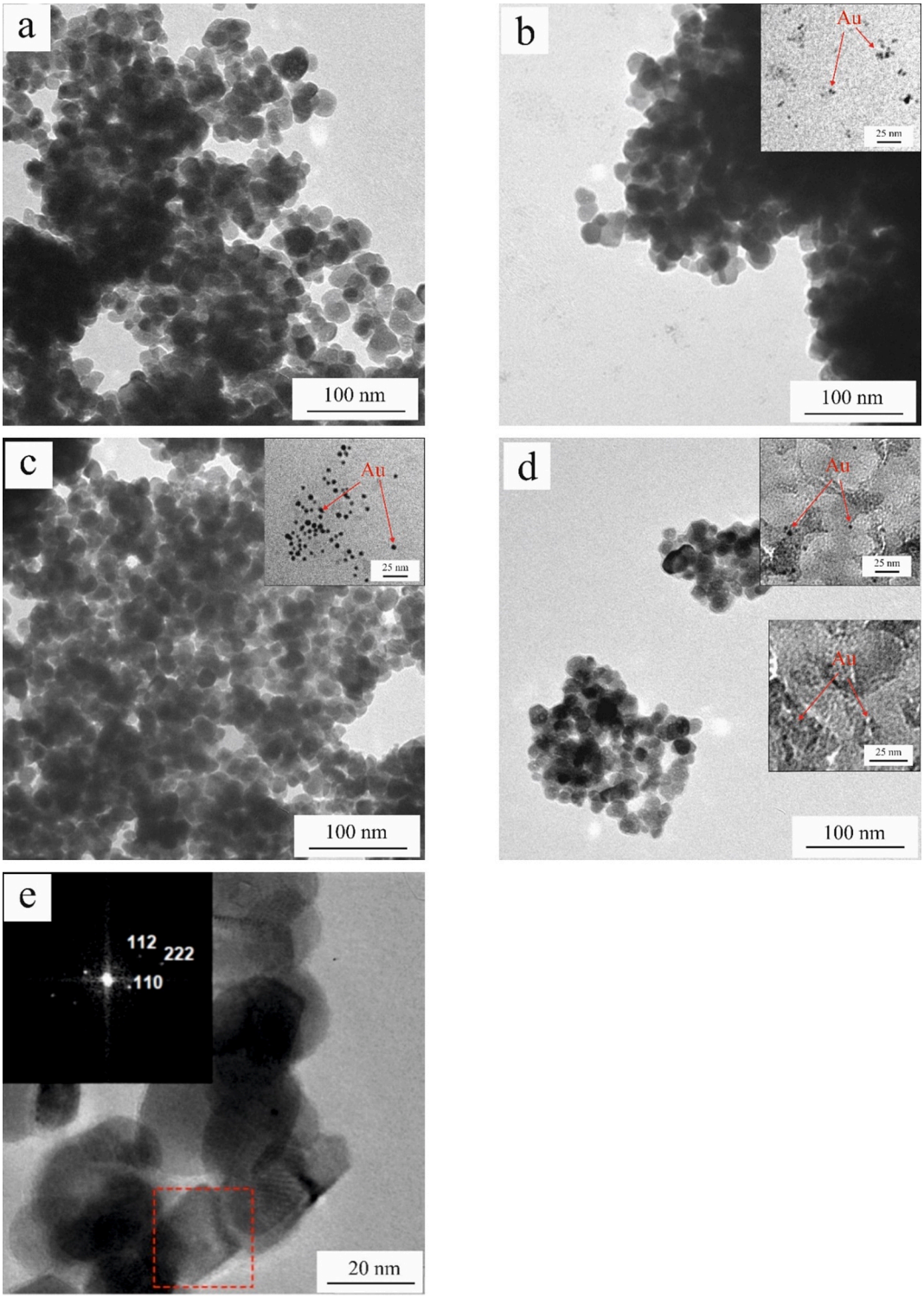

Fig. 3. TEM images of samples: In_2O_3 (*a*); In_2O_3–Au,*Tet* (*b*); In_2O_3–Au,*Cit* (*c*); In_2O_3–Au^{III} (*d, e*); In_2O_3–Au^{III} (*e*) and AuNPs in them. The inset images: in (*b*) – AuNPs particles detached from the In_2O_3 surface; in (*c*) – colloidal AuNPs,Cit particles; in (*d*) – particles after etching of In_2O_3 in HNO_3 ; in (*e*) – electron diffraction from an selected area.

Table 2
Grain size of In_2O_3 and AuNPs acquired by TEM and other methods.

Sample No	1	2	3	4
Designation	In_2O_3	In_2O_3–Au,*Tet*	In_2O_3–Au,*Cit*	In_2O_3–Au^{III}
d_{In2O3}, nm	18.5	14.5	14.5	14.5
d_{Au}, nm		1.5	3.5 nm	1.5

In_2O_3–Au,*Cit* and In_2O_3–Au^{III}, as well as their slight difference from the spectrum of In_2O_3. The lines related to surface hydroxyl groups are less intense in the spectra of the In_2O_3–Au samples in comparison with In_2O_3. In case of In_2O_3–Au,*Tet*, there is a growth of intensity of these lines, which might be due to the effect of sulfate groups that emerge on the surface of In_2O_3 after the decomposition of mercaptoethyltetrazole. It is known that the resulting SO_3 molecules are adsorbed on the surface

Table 3
Electron diffraction parameters of In_2O_3–Au^{III} (0.2 wt% Au) sample.

$d_{measured}$, Å	C-In2O3 JCPDS06-0416			R-In2O3 JCPDS 21–0406			Au JCPDS 02–1095		
	d, Å	Irel, %	h k l	d, Å	Irel, %	h k l	d, Å	Irel, %	h k l
2.90	2.92	100	222	2.885	100	104			
2.54	2.529	30	400	–					
2.35	2.385	8	411	2.384	20	113	2.36	100	111
2.24	2.262	2	420	2.255	10	202			
2.13	2.157	6	332	–			2.04	90	200
1.97	1.984	10	431	1.985	70	24			
1.78	1.788	35	440	1.814	60	116			

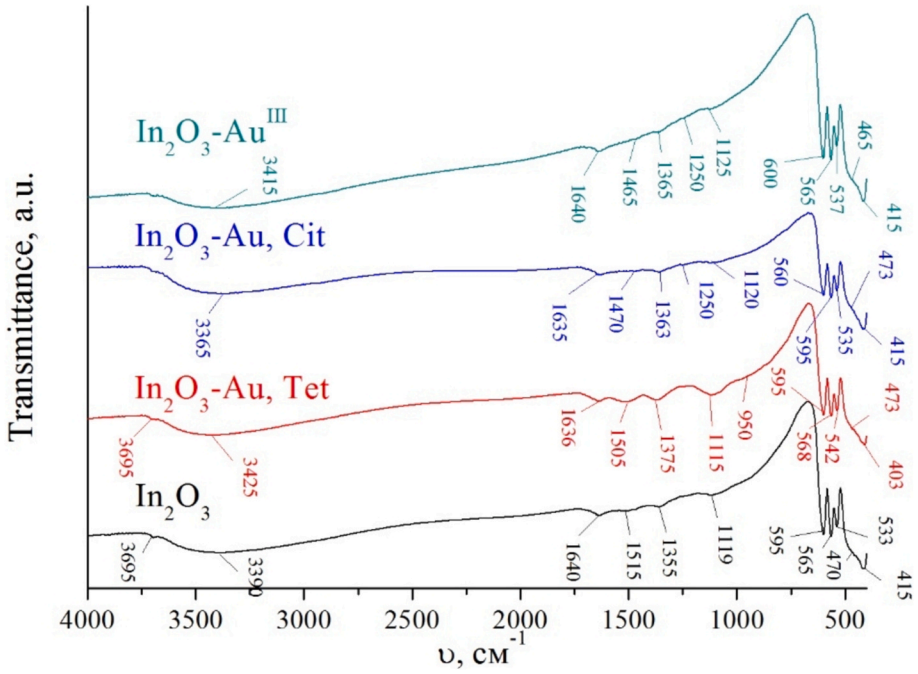

Fig. 4. IR spectra of In_2O_3; In_2O_3–Au,*Tet*; In_2O_3–Au,*Cit*; In_2O_3–Au^{III} samples.

Table 4
Bands (cm^{-1}) registered in IR spectra of In_2O_3 and In_2O_3–Au samples.

In_2O_3	In_2O_3–Au,*Tet* 1.5 nm	In_2O_3–Au,*Cit* 3.5 nm	In_2O_3–Au^{III} 1.5 nm	Assignement
415	403	415	415	ν(In–O)
470^{sh}	473^{sh}	473	473 465	
533	542	535	537	ν(In–O)
565	568	560	565	
595	595	595	595 600	
	950^{sh}1115			$\nu_1(S–O/SO_4^{2-})$
1119	1115	1120^{w}	1120^{w}	ν_3(In–O–H)
			1250^{vw}	$\nu_1(CO_3H)$
1355	1375	1363	1365^{vw}	ν_s(–OCO–)
1515	1505	1470^{vw}	1465^{vw}	ν_{as}(–OCO–)
160	130	107	100	$\Delta = \nu_{as} - \nu_s$
1640	1635	1635	1640	δ(H − O − H)
3390	3425	3365	3415	ν(OH…H_2O)
3695	3695			ν(O–H)

^{sh} – shoulder, ^{w} – weak, ^{vw} – very weak.

of the oxide, causing a change in the state of metal cations and hydroxyl groups [54,55]. This phenomenon has been revealed for many metal oxides used in catalysis, including tin dioxide [31]. The occurrence of adsorbed SO_x molecules causes a change in the frequency of In–O vibration observed in the spectrum of In_2O_3–Au,*Tet*, thereby changing the electron-acceptor properties of metal ions in the oxide.

Electron paramagnetic resonance. In the spectra of the samples recorded at 298 K, only a triplet signal characteristic of •NO_2 radicals is registered with the parameters as follows: $g_{av} = 2.003$, $A(^{14}N) = 5.5$ mT (nuclear spin $I(^{14}N) = 1$) (Fig. 5a) [56,57]. Nitrate ions captured within the polymer structure of indium hydroxide at the stage of sol formation might be preserved in the form of NO_2 in In_2O_3 up to 600 °C [57]. In the spectra of all samples recorded at 77 K (Fig. 5b), a broad signal with the parameters indicated in Table 5 is emerged along with the triplet signal of •NO_2 with $g_{av} = 2.002$, $A(^{14}N) = 5.7$ mT. No evidence of •NO_2 traces was found in In_2O_3 sample heated at 800 °C as seen in Fig. 5 (spectrum 5). The acquired signal reflects the shape of the resonance line with $g_{av} \sim 2.056 \pm 0.006$ with no distortion arisen from •NO_2 radicals. This signal appears in the EPR spectra of indium oxide after heating at 500 °C, reaches its maximum intensity at 800 °C, and preserves up to 900 °C [57].

The signal at $g_{av} \sim 2.056 \pm 0.006$ found in the spectra of samples 1, 3 and 4 differs slightly in intensity, width (ΔB) and *g*-factor. All the parameters are increased in case of sample 2 only. These changes might be caused by the effect adsorbed SO_x^- groups, changing the donor–acceptor properties of metal cations on the surface of In_2O_3 [54]. Their formation and adsorption are the result of thermal decomposition of mercaptoethyltetrazole. Adsorption of SO_2 molecules can change the relaxation parameters and spin-exchange interactions, thereby affecting the intensity and width of the signal. It worth noting that in the case of wide signals, the broadening of which can be caused by various reasons (some will be discussed below), their parameters (intensity and width) are not related to the concentration of spins. This is particularly true for

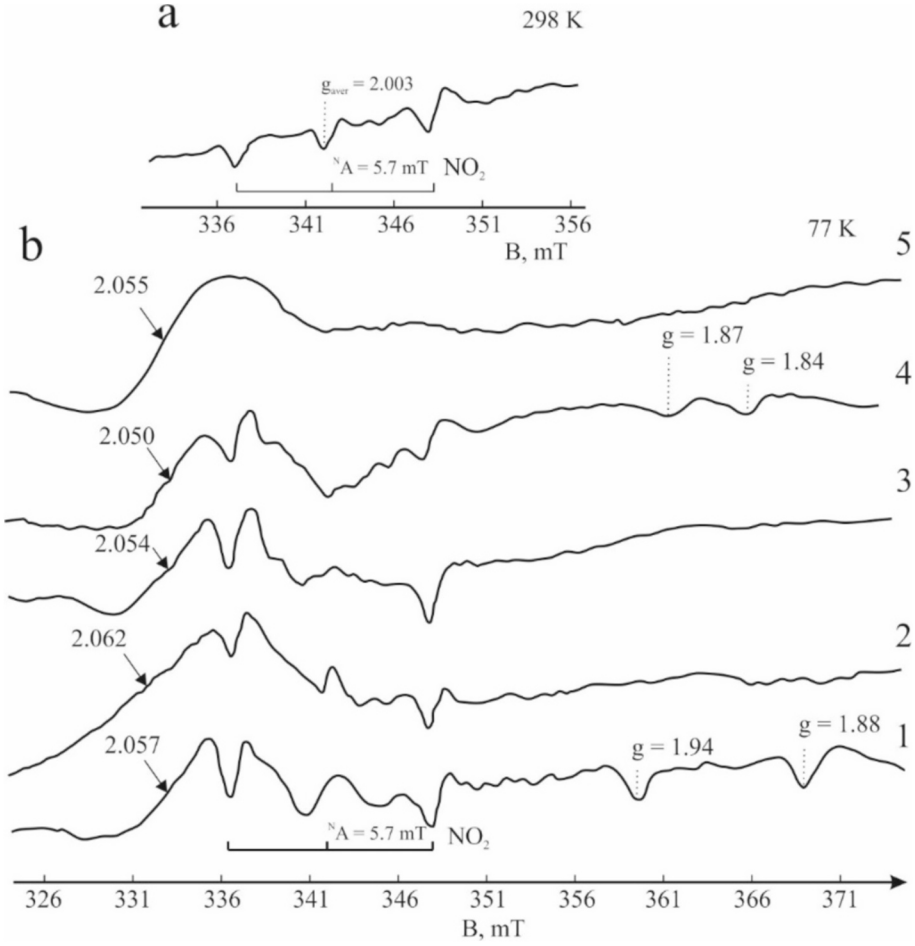

Fig. 5. EPR spectra recorded at 298 K (a) In_2O_3 and at 77K (b): 1 – In_2O_3; 2 – In_2O_3–Au,Tet; 3 – In_2O_3–Au,Cit; 4 – In_2O_3–Au^{III} ; 5 – In_2O_3. Samples 1–4 are annealed at 600 °C, sample 5 – at 800 °C.

Table 5
EPR spectroscopy data acquired from In_2O_3 and In_2O_3–Au samples at 77 K.

Sample	•NO_2	g_{av}, O^-	ΔB, mT, O^-	I_{rel}, O^-	Other paramagnetic centers, ($V_O^{\bullet}$)
In_2O_3	g = 2.003	2.057	5.5	1.0	1.94; 1.88
In_2O_3–Au, *Tet*	g = 2.003	2.062	11.5	1.68	
In_2O_3–Au, *Cit*	g = 2.003	2.054	5.5	0.95	
In_2O_3–Au^{III}	g = 2.003	2.050	5.5	0.91	1.87; 1.84

complex centers in which electron exchange between components is possible.

Low intensity signals with $g < g_e$ can be assigned to such centers as electron captured by oxygen vacancy ($V_O^{\bullet}$). The value of *g*-factor is predetermined by the symmetry of the coordination environment (field potential).

A broad signal with a high value of $g \gg g_e$, similar to our signal with $g_{av} \sim 2.056 \pm 0.006$, was observed in the spectra of various oxides (MgO, MoO_3, ZrO_2) and attributed to O^- hole centers [58–61]. Hole centers have a short lifetime in conducting matrixes since they capture electrons quickly according to the equation: $O^- + e \rightarrow O^{2-}$ [58] For this reason, their registration is not always possible in well-conducting oxides. However, they are detected in amorphous (GeO_2) [58,59] and non-conducting oxides (ZrO_2, MgO) as "unbound" oxygen O^- [58,60]. The registration of similar centers in photoactivated TiO_2 is favored by the presence of titanium vacancies in the lattice [61]. One can assume that the detection of O^- in *C*–In_2O_3 at 77 K also becomes possible due to the occurrence of other defects. Interstitial indium ions [In_i] as well as cation vacancies V_{In} are the defects typical of *C*–In_2O_3 crystal lattice. The mentioned defect could stabilize O^--centers.

Based on the measurements of electrical properties, the authors of [55,62,63] concluded that the high quasi-metallic conductivity in indium oxide is caused by indium ions in low oxidation states, oxygen vacancies (V_O), and interstitial indium ions [In_i]. Their formation occurs according to the equations as follows:

$$[O_o]^{2-} \leftrightarrow V_o + 2e + 1/2O_2 \quad (1)$$

$$2[In_{In}]^{3+} + 3[O_O]^{2-} \leftrightarrow 2[In_i]^{3+} + 3V_O + 6e + 3/2O_2 \quad (2)$$

The conduction electrons being formed in In_2O_3 can be delocalized in the crystal lattice in the conduction band formed by the 5 *s* orbitals of indium. Also, they can be captured by both single In^{3+} ions and oxygen vacancies *Vo* resulting in In^{2+} ions and $Vo^{\bullet}$ (F^+-centers), respectively. The shift of indium to the interstitial site leads to the formation of V_{In} vacancy. Some authors [38,46] suppose that the high electrical conductivity of In_2O_3 at temperatures lower than 550 °C is due to the ease of electron exchange between different states of indium: $2In^{2+} \leftrightarrow In^+ + In^{3+}$, $\Delta G = 0$. The band mechanism of charge transfer is realized as a result of overlapping levels of In^{2+} (5 s^1) and In^+ (5 s^2) [37,62].

Hole centers play an important part in the formation of In^{2+}, since this state is formed by trapping holes in more stable In^+ sites (5 s^2 states). Under certain conditions, e.g. in the presence of defects in crystal structures (like cation vacancies V_{In}), a stabilization of these In^{2+} states,

which are unstable under normal conditions, is possible. The formation of In^{2+} and O^- sites in In_2O_3 is an interconnected process. They are formed together with a cation vacancy, which prevents the recombination of centers with donor and acceptor properties: $In^{2+} + O^- \rightarrow In^{3+} + O^{2-}$. Thus, the signal at $g_{av} \sim 2.056 \pm 0.006$ is an attribute of the complex center referred to as In^{2+}–O^-–V_{In}. The high signal width might be due to the unresolved hyperfine structure (10 lines) from the interaction of the spin density with the magnetic moment of the neighboring ^{113,115}In ion, which has a nuclear spin of 9/2. The similar type centers being a combination of In^{2+} and V_{Zn} were previously revealed in In/ZnS materials [64]. The described complexes are capable of participating in electron transfer in case of metal cations with variable valence. This combination of donor and acceptor ions ensures reversibility of the process, stability and reproducibility of the sensory response on indium oxide [65]. Hole O^- centers have an increased reactivity in the range of 150–450 °C, in which most gases are typically detected. The surface of AuNPs is expected to be activated with O^- sites by partial transferring electron density between them [34,35,66]. This explains the slight decrease in the intensity of the O^- EPR signal in In_2O_3–Au, *Cit* or In_2O_3–Au^{III} samples as compared to pure In_2O_3.

The quantum size effect in gold clusters with a size of 1.5–3 nm leads to a decrease in the electron density of *d*-levels due to a partial transfer of

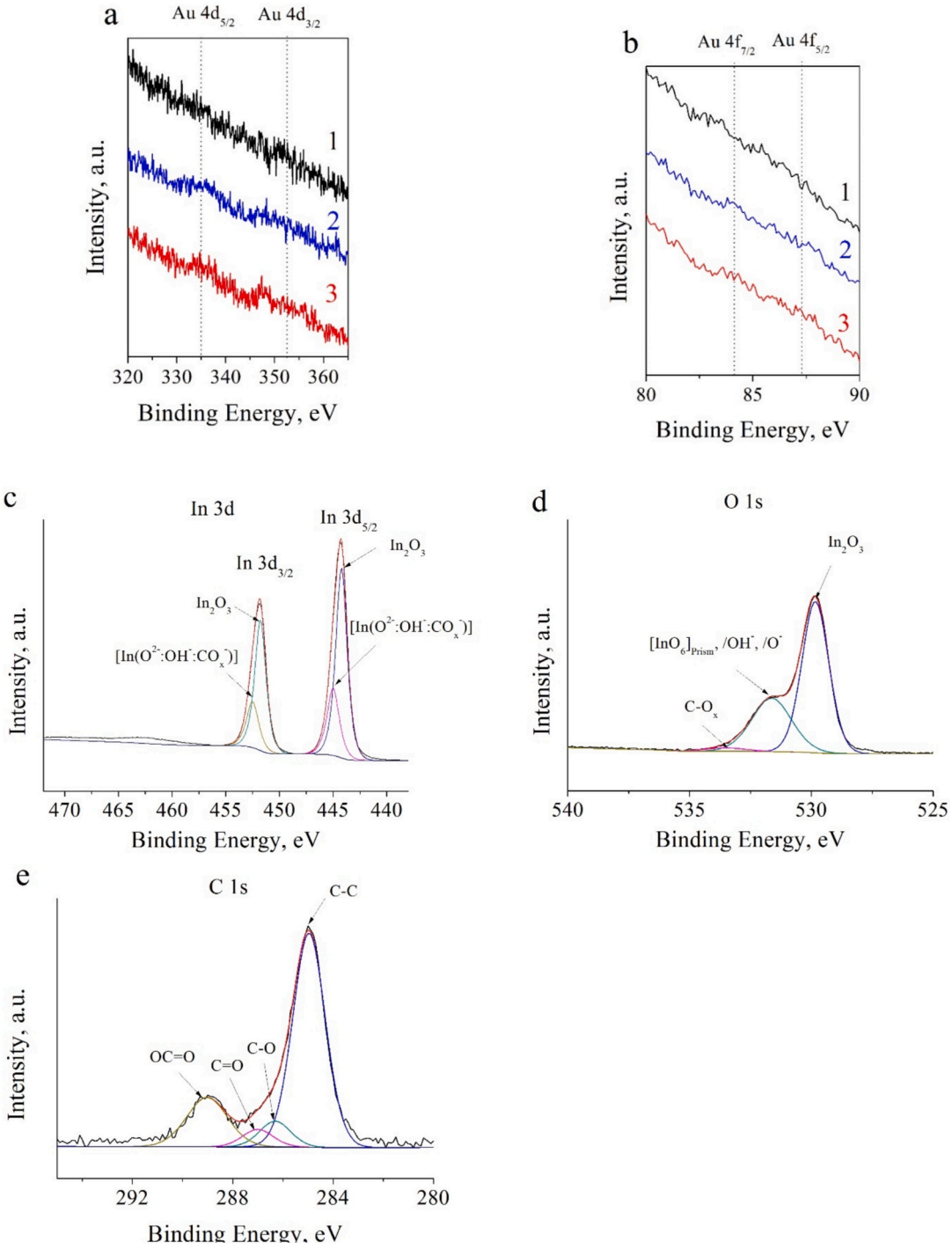

Fig. 6. Au 4*d* (*a*) and Au 4*f* (*b*) XPS spectra of the In_2O_3–Au,*Tet* (1), In_2O_3–Au,*Cit* (2), In_2O_3–Au^{III} (3); In3*d* (c), O1*s* (d) and C1*s* (e) lines in the XPS spectra of In_2O_3 sample.

the electron density from the *d*-orbital to the *p*-orbital: $[d^{10}s^1] \rightarrow [d^8s^1p^2]$ [3]. Such a change in the filling the orbitals in clusters promotes the interaction of gold with oxygen and its activation [67]. Due to the low concentration of gold, we did not detect the formation of gold cluster complexes with oxygen using the EPR method, although this effect is observed in In_2O_3–Au samples with a higher gold concentration (0.5 wt %).

There is a correlation between the occurrence of oxygen deficiency (oxygen vacancies) on the surface of indium oxide and the content of surface hydroxyl groups and O^- centers. Both oxygen vacancies and O^- sites emerge under thermal dehydration of indium hydrosol. Their formation from hydroxyls can be represented by the schemes as follows [58]:

$$OH^- + OH^- \rightarrow O^- + H_2O + e \quad (3)$$

$$2OH^- \rightarrow O^{2-} + H_2O + V_O \quad (4)$$

The O^- centers are also produced under thermal decomposition of nitrate ions, which are introduced a sol in form of nitric acid as a stabilizer:

$$NO_x^- \rightarrow O^- + N_2O \rightarrow O^- + N_2 \quad (5)$$

In accordance with one of the declared mechanisms of acetone detection, an important role of O^--centers in the oxide is emphasized [24,25]. The presence of O^- is also important for the activation and detection of CO. These can be either ionically sorbed or lattice O^--centers.

X-ray photoelectron spectroscopy. In3*d*, O1*s* and C1*s* lines in the XPS spectra of In_2O_3 and In_2O_3–Au samples differ slightly. Therefore, the In3*d*, O1*s* and C1*s* spectra recorded from In_2O_3 sample are only depicted in Fig. 6, c-e. The results are analyzed and summarized in Table 6.

In 3*d* и O1*s* spectra recorder from In_2O_3 or In_2O_3–Au samples are typical of indium oxide [66, 657 The single-shaped In 3*d* lines are separated into two components of approximately equal width (*FWHM* 1.24 and 1.33 eV) with binding energies (*BE*) listed in Table 6. Higher intensity line with *BE* In $3d_{5/2}$ = 444.2 eV is undoubtedly attributed to In^{3+} in In_2O_3 [66]. Taking into account the high dispersity of In_2O_3, the state with 445.0 eV might be assigned to near-surface In^{3+} sites coordinated with various ions like O^{2-},OH^- and CO_x^- giving rise to [In(O^{2-}:OH^-:CO_x^-)] complex. The occurrence of surface O^- centers in the coordination environment of In^{3+} would also contribute to this peak.

Two states of oxygen with a small admixture of a third state are distinguished in O 1 s spectra (see Table 6). The chemical nature of the second peak of lower intensity but greater width (*FWHM* 1.92 eV) might be complex. Different forms of oxygen can contribute into the signal: OH^-, O^-, O_{lat}^{2-} in non-stoichiometric surface layers [66,67]. However, according to some researchers, two peaks in the O 1 s spectrum of the cubic phase *C*–In_2O_3 are attributed to lattice oxygen in the coordination of an octahedron or a prism.

In the spectra of In_2O_3 and In_2O_3–Au, the quantitative difference between the In 3*d* and O 1 *s* peaks is insignificant. An increase in the content of surface oxygen in the spectrum of In_2O_3–Au,*Tet* and a decrease in case of In_2O_3–Au,*Cit* is observed in comparison with In_2O_3 sample. This change may be due to the effect of thermal decomposition products of the introduced gold stabilizers on the state of indium oxide surface. Due to a small amount of gold and stabilizer being introduced, the effect is not pronounced. The discussed XPS results are consistent with the above IR and EPR data supporting the increased content of OH^- and O^- in In_2O_3–Au,*Tet*.

Weak N 1 s lines with *BE* = 400 eV are registered in the spectra of all samples under study. They are evidently attributed to N–C bonds, which encounter in different types of compounds. In particular, the indicated *BE* value is characteristic of pyrrole type nitrogen. According to the relative intensity of N 1 s peaks (indicated in parentheses), the samples are arranged in a row:

In_2O_3 (2) > In_2O_3–Au^{III} (1.6) > In_2O_3–Au,*Tet* (1) > In_2O_3–Au,*Cit* (0.8)

As follows from the XPS data, the presence of gold particles reduces the efficiency of formation and adsorption of (– N < C) structures on the surface of indium oxide.

The oxidized state of nitrogen (NO_2), which was revealed by EPR, is not detected on the surface of the samples by XPS method. This confirms NO_2 fixation in the bulk of indium oxide.

Low-intensity S $2p_{3/2}$ and S $2p_{1/2}$ lines with *BE* = 169 and 174 eV are registered in spectrum of In_2O_3–Au,*Tet*. They are characteristic of SO_4^{2-} state [54,66].

Neither Au 4*f* nor Au 4*d* lines are emerged in XPS wide-scan spectra due to the low gold concentration. Increasing the magnification level allowed detecting very weak Au 4*f* and Au 4*d* lines. The spectra are shown in Fig. 6, a, b. The position of the maxima corresponds to the Au state (marked with dash lines). Poor resolution of the Au4*f* and Au4*d* lines, which is due to their broadening and low intensity, confirms the high dispersion of gold in the samples and does not allow evaluating the features of the electronic state of the AuNPs surface with complete certainty. It can be assumed that the large line width might be a consequence of the inhomogeneity of the state of gold atoms on the AuNPs surface [68]. It can be noted that in the Au4*d* spectra of In_2O_3–Au,*Cit* and In_2O_3–Au^{III} samples, a decrease in the value of Δ = Au$4d_{3/2}$ – Au$4d_{5/2}$ is observed relative to metallic gold, which is evidently a consequence of a decrease in the electron density in the *d*-orbitals, which is very characteristic of particles of this size. Gold clusters with the sizes of 1.5–3 nm are characterized by rather molecular bonds than metallic ones [2,3,6].

3.2. Results of sensor measurements

Electrical resistance. The temperature-dependent resistance and response of the sensors to CO and CH_4 are depicted in Fig. 7a, b, c. As follows from Fig. 7a, all Au-doped In_2O_3 sensors have maximum

Table 6
Results of analysis of XPS wide-scan spectra recorded from In_2O_3 and In_2O_3–Au.

Sample	In_2O_3		In_2O_3–Au,*Tet*		In_2O_3–Au,*Cit*		In_2O_3–Au^{III}	
Parameters	BE, eV	%	BE, eV	%	BE, eV	%	BE, eV	%
O 1*s*/$[InO_6]_{Oh}$	529.8	34.7	529.8	34.9	529.9	35.9	529.9	35.6
$[InO_6]_{Prism}$, /OH^-, /O^-	531.6	18.2	531.6	20.1	531.7	18.4	531.8	18.4
CO_x	533.5	1.1	533.2	0.6	533.2	1.2	533.6	0.9
In $3d_{5/2}$/In_2O_3	444.2	23.3	444.2	23.4	444.3	22.3	444.3	22.4
[In(O^{2-},OH^-, CO_x^-)]	445.0	8.5	445.0	7.8	445.0	9.9	445.0	9.4
C 1*s*, C–C	285.0	10.2	285.0	8.7	285.0	7.1	285.0	8.1
C–O	286.3	1.2	286.3	0.8	286.0	1.5	286.3	1.7
C=O	287.0	0.8	287.0	1.0	287.0	0.8	287.0	0.7
OC=O	289	3.0	289	2.9	289	2.9	289	2.9
N 1*s*/–N<C	400.0	<1	400	<1	400.0	<1	400.0	<1
S $2p_{3/2}$/SO_4^{2-}			169	<1				

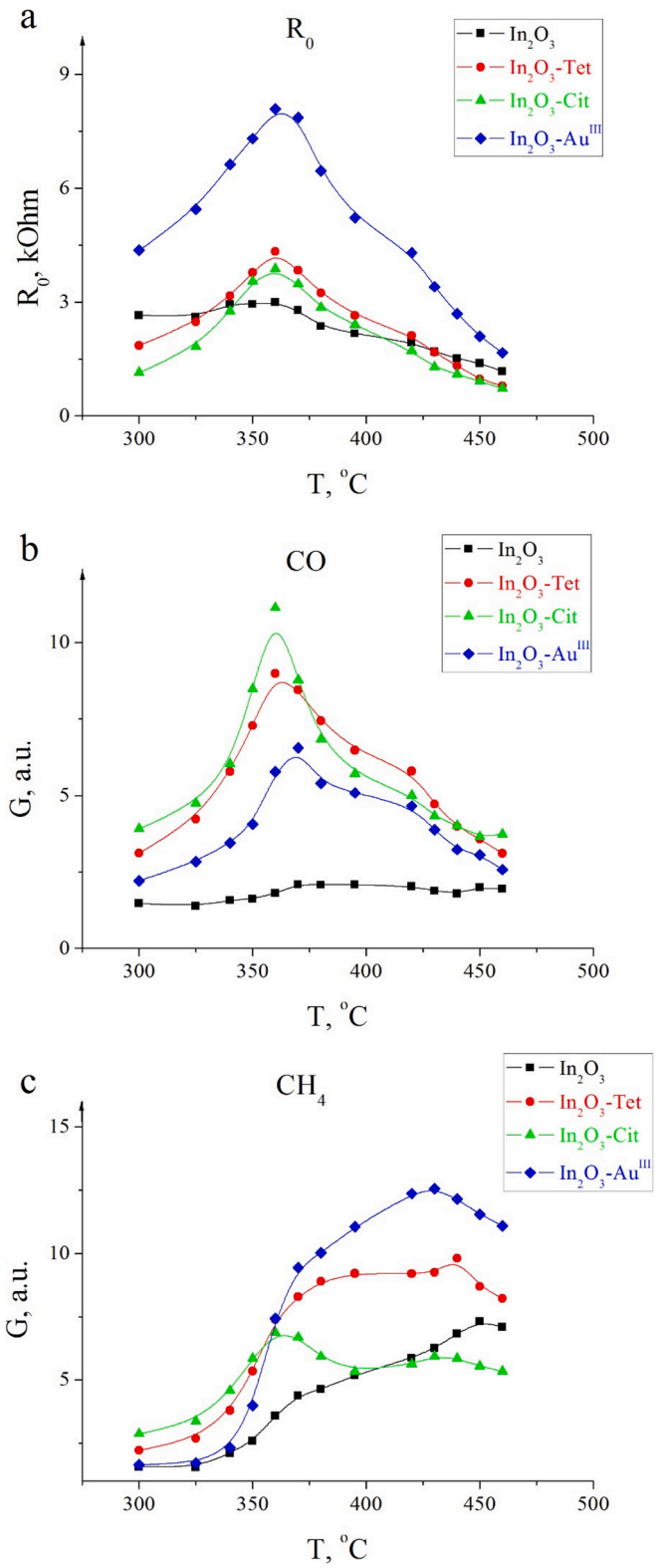

Fig. 7. Effect of working temperature on electrical resistance (R) (a) and response (G) of sensors to CO (b) and CH_4 (c).

electrical resistance (at 360 °C) higher than that of pure In_2O_3 sensors. The greatest increase in resistance over the entire temperature range (300–470 °C) was measured for the sample when gold was introduced in form of Au^{III} ions. The resistance of all layers displays only minor difference at low (300–320 °C) or high (420–470 °C) temperatures. The greatest increase in the electrical resistance within the entire temperature range (300–470 °C) occurs with the introduction of Au^{III} ions.

The observed changes in the electrical resistance of In_2O_3–Au layers can be explained by taking into account the temperature dependence of the electrical conductivity of indium oxide. Indium oxide is a typical semiconductor with impurity conductivity at low temperatures (up to 200 °C), intrinsic conductivity at high temperatures (400–600 °C) and a conductivity saturation region between them, the position of which can vary [37,69]. The observed maximum resistance of In_2O_3–Au sensors is in the temperature range corresponding to In_2O_3 saturation region of conductivity and its slight decline in the range of 280–400 °C [69].

An increase in the resistance of semiconducting metal oxides when modified with noble metal is typical and has been observed previously [34,36]. The reasons for the increase in the resistance of oxide composites in the saturation temperature region when modified with noble metals might be a decrease in the effective concentration and mobility of free charge carriers. At $T \geq 300$ °C, surface oxygen vacancies are supposed to be effective donor conduction centers in the structure of most n-type semiconductor oxides [37,62]. The presence of AuNPs can affect the number of such conduction centers as well as their mobility, making current transport more difficult.

One can assume that the substantial growth of resistance in sample 4 within a large temperature range might be a result of creation of energy barriers at the grain boundaries of In_2O_3 due to the distribution of gold atoms over them.

Sensitivity to CO and acetone. As follows from Fig. 7b, the response to CO of In_2O_3 oxide increases significantly when modified with gold. The magnitude of the response values decreases in the row:

$$In_2O_3\text{–Au},\mathit{Cit} > In_2O_3\text{–Au},\mathit{Tet} > In_2O_3\text{–}Au^{III} > In_2O_3$$

The maximum response signal corresponds to temperature of 360 °C, at which the electrical resistance reaches its maximum (see Fig. 7a, b), with a slight shift in the position of the maximum (370 °C) in case of In_2O_3–Au^{III} and In_2O_3 layers. One can note the narrow temperature range of effective detection of CO in case of In_2O_3–Au sensors and the weak dependence of the response of pure In_2O_3 layer to CO on working temperature.

The behavior of the studied sensors to acetone is similar to that revealed for CO. The temperature dependence of similar In_2O_3–Au and In_2O_3 sensors was studied earlier [70]. It was shown that no shift in the position of the maximum of the response signal is observed upon the introduction of gold. An increase in the response value was only revealed. The sensitivity of the sensors to CO and acetone are comparted together in Fig. 8. The evident correlation in changes of the response of

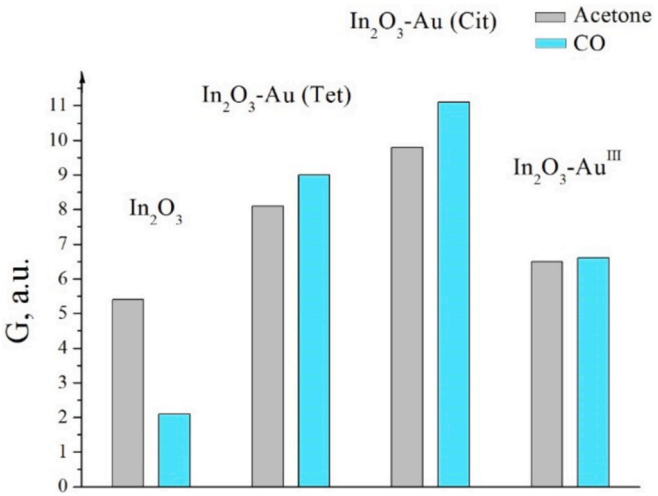

Fig. 8. Comparison of sensitivity of In_2O_3 and In_2O_3–Au sensors when detecting 100 ppm of CO (T = 350 °C) and 10 ppm of acetone (T = 325 °C).

In_2O_3–Au sensors to CO and acetone might be a consequence of the similarity of their detection mechanisms in the range of 300–400 °C. The temperature range of the maximum response of the In_2O_3–Au sensors coincides with the region where the reaction of catalytic oxidation of CO proceeds effectively on In_2O_3 oxide. Using the method of temperature-programmed catalysis, it was found that the maximum conversion of CO with the release of H_2O and CO_2 occurs at 350–400 °C [69]. Consequently, AuNPs increase the efficiency of catalytic oxidation on the surface of In_2O_3, promoting the activation of oxygen O^{2-} at the In_2O_3/Au interface. Acetone is detected by the same oxidation–reduction mechanism [44]. Using ^{16}O and ^{17}O isotopes, it has been shown the important role of surface O^{2-} ions of metal oxide in the mechanism of catalytic oxidation of CO [20,21,45,65]. We did not observe a decrease in the detection temperature of CO and acetone by In_2O_3–Au sensors in the low temperature region, where another detection mechanism could be realized [31,32]. One of the reasons for this may be the low concentration of gold.

The response values of the layers to CO and acetone have been found to correlate with the size of the AuNPs. The maximum output signal of the In_2O_3–Au sensors is achieved at $d_{Au} = 3.5$ nm. With the same AuNPs size of about 1.5 nm, the response of the In_2O_3–Au,*Tet* sensor is higher than that of In_2O_3–Au^{III}. This can be explained by the different technology of obtaining these samples, which leads to different arrangement of AuNPs in them. Sulfate (SO_4^{2-}) groups, as well as a higher concentration of OH groups, can have a positive effect on the adsorption properties of In_2O_3–Au,*Tet*.

The maximum degree of CO conversion to form CO_2 is observed at 350 °C. There is a clear correlation between the oxidation process and the change in the electrical conductivity of the oxide or sensor.

The previously established sensitivities of SnO_2–Au sensors to CO and acetone are placed in the rows as follows [31]:

CO: SnO_2–Au,*Cit* > SnO_2–Au,*Tet*; SnO_2–Au^{III} > SnO_2.

Acetone: SnO_2–Au,*Cit* > SnO_2–Au,*Tet* > SnO_2–Au^{III} > SnO_2.

The same dynamics of the response of In_2O_3–Au and SnO_2–Au sensing layers is observed, which shows the similarity of factors influencing the characteristics of these sensors when detecting CO and acetone. The results obtained on the response of In_2O_3–Au and SnO_2–Au sensors to CO are in accordance with the data reported in [6] and [11] where a great importance of AuNPs size had been revealed. The highest activity of gold with $d_{Au} = 3.5$ nm as compared to $d_{Au} < 2$ nm was shown. It has been noted [14] that an optimal ratio between the surface Au atoms and the atoms located at the Au/oxide (TiO_2) boundary is typical of gold particles with $d = 3.5$ nm. At temperatures higher than 300 °C, the activation of CO and O_2 proceeds at the Au/oxide interface.

To date, the most cited model of the mechanism of acetone or CO detection by resistive metal oxide sensors assumes the interaction of gas molecules with ionically adsorbed forms of O^- [24,25]. However, this is not the only mechanism of detection of both CO and acetone [24,43,44]. On some oxide materials with high sensitivity to acetone, such forms of oxygen do not exist [43,44]. Moreover, it has been shown that the detection of acetone or CO, is possible even in the absence of oxygen in the gas phase [43–45]. Therefore, other mechanisms are proposed to explain the observed phenomena. It has been shown that detection of acetone, as well as CO, can be realized by the oxidation–reduction mechanism of the so-called "oxygen-vacancy model" [44]. Using Combined Operando UV/Vis, Raman, and IR Spectroscopy, it was shown that the response of SnO_2 sensors to ethanol correlates directly with the number of surface oxygen vacancies and the occurrence of surface acetate and hydroxyl groups [46]. The similarities in the mechanisms of acetone and ethanol detection are observed [24,25]. The correlation in the change in the response of In_2O_3–Au sensors to CO and acetone may indicate the similarity of their detection mechanisms in the temperature range of 325–360 °C. A relation was found between the degree of CO conversion and the change in the electrical conductivity of indium oxide, the maximum change in these parameters is observed at 350–400 °C [69]. This result also suggests an oxidation–reduction mechanism involving lattice oxygen and the formation of oxygen vacancies. At the first stage, oxygen is activated, and then gas molecules are oxidized as follows:

$$[In^{3+}\text{–}O^{2-}]_{lat} \rightarrow [In^{2+}\text{–}O^{-}]_{lat}; \quad (6)$$

$$CO_{ads} + [O^-]_{surf} \rightarrow CO_{2gas} + V_O + e; \quad (7)$$

$$CH_3COCH_{3ads} + [O^-]_{surf} \rightarrow CH_3CO_{ads} + CH_3O_{ads} + V_O + e. \quad (8)$$

The increase in the efficiency of the detection process with the introduction of Au can be due to the activation of oxygen and CO along the perimeter of AuPNs in the area of contact with In_2O_3 [34,35]. The participation of AuPNs in the process changes the number and nature of gas adsorption centers, thereby enriching the In_2O_3–Au surface with active oxygen forms.

In case of In_2O_3, oxygen activation can also occur on In^{2+} ions, which, together with oxygen vacancies, occurs in non-stoichiometric indium oxide:

$$In^{2+}_{surf} + O_{2ads} \rightarrow In^{3+}_{surf} + O^-_{2ads}; \quad (9)$$

$$O^-_{2ads} + [e] \rightarrow 2O^-_{ads}. \quad (10)$$

It should be kept in mind, however, that the O^- hole centers, detected by EPR method, can also participate in the detection reaction on indium oxide. Due to their high activity, surface [O^-] hole centers can themselves participate in the oxidation of gas molecules or activate adsorbed oxygen. The participation of hole centers can be represented in the form of equations as follows:

$$[O^-]_{surf} + CO_{ads} \rightarrow CO_{2gas} + V_O + [e]_{bulk}; \quad (11)$$

$$[O^-]_{surf} + O_{2ads} \rightarrow O^-_{2surf} \text{ (complex of } O^- \text{ with } O_2 \text{ on } In_2O_3 \text{ surface)}; \quad (12)$$

$$CO_{ads} + O^-_{2surf} \rightarrow CO_{2gas} + O_{2gas} + V_O + [e]_{bulk}; \quad (13)$$

Adsorption of oxygen leads to re-oxidation of the oxide surface:

$$[e]_{bulk} + O_{2ads} \rightarrow O^-_{2ads}; \quad (14)$$

$$O^-_{2ads} + [e]_{bulk} \rightarrow 2O^-_{surf}. \quad (15)$$

$$O^-_{surf} + [e]_{bulk} \rightarrow O^{2-}_{surf}. \quad (16)$$

Sensitivity to methane. The introduction of gold into indium oxide increases its sensitivity to methane (Fig. 7c). However, the response of the In_2O_3–Au sensors as a function of temperature is more complex than in case of CO. One can distinguish two temperature ranges of detection as seen from Fig. 7c. Within the range of 200–400 °C the electrical conductivity of indium oxide reaches saturation, while at higher temperatures the conductivity changes exponentially with an activation energy (E_{act}) higher (0.18–0.20 eV) than in the region of impurity conductivity ($E_{act} = 0.1$ eV up to 200 °C) [69]. The low response maximum is observed at the same temperature (360 °C) as the maximum to CO. At this temperature, all In_2O_3–Au sensors demonstrate similar magnitudes of the signal to CH_4. Therefore, one can assume a similarity in the mechanisms of CO and methane detection at this temperature. This assumption follows from the previously established correlation between the processes of CO and CH_4 conversion, as well as from the change in the electrical conductivity of indium oxide in air and in the presence of the gas [57,69].

The second maximum is observed for the Au-containing layers at temperatures (415–440 °C) slightly lower than for In_2O_3 (450 °C). This temperature range corresponds to the intrinsic conductivity of indium oxide [35,67]. It was previously shown that the highest growth of the electrical conductivity of indium oxide in the presence of methane is observed at 450 °C when CH_4 conversion reaches its maximum [69]. This fact allows us assuming that at 415–450 °C, methane detection is

realized through the mechanism of alternating oxidation–reduction with the participation of lattice oxygen O^{2-} according to quazi-equation (6).

High temperature is necessary to activate oxygen and break the strong C–H bond in CH_4 [71]:

$$CH_4 \rightarrow CH_3 + H; \quad (17)$$

Further transformation of methyl groups by different mechanisms is possible. In [21] the following scheme is proposed:

$$CH_3 + H + 4[O^-] \rightarrow CO_2 + 2H_2O + 4V_o + 4e. \quad (18)$$

At 400 °C, the process probably proceeds according to scheme 18. However, at lower temperatures, reactions with the formation of intermediate products are possible, for example, as follows [72]:

$$CH_3 + CH_3 + O_{lat} \rightarrow CH_3CH_2O_{lat} + H_{ads}; \quad (19)$$

$$CH_3CH_2O_{lat} + H_{ads} \rightarrow H_2O_{gas} + C_2H_{4gas} + V_o. \quad (20)$$

The adsorbed oxygen re-oxidizes the formed oxygen vacancies according to reactions (14) (15) (16).

An unexpectedly high output signal is registered in case of In_2O_3–Au^{III} sensor in contrast to the other In_2O_3–Au layers or to SnO_2–Au^{III}. The introduction of Au^{III} into SnO_2 sol does not affect the sensitivity to methane as shown in [31]. Apparently, the high response of In_2O_3–Au^{III} sensors to methane may be due to a specific state of AuPNs in this sample, which significantly reduces the electrical conductivity in the polycrystalline In_2O layer. To explain the significant increase in resistance and the growth of the response to methane in the high-temperature region, a model can be used that assumes the formation of a Schottky barrier at the In_2O_3 grain interface, which hinders current transfer in the contact region of indium oxide grains. The AuPNs can create this type of local energy barriers in indium oxide at In2O3 grain boundaries if they are distributed at the edges and steps of the lateral faces of In_2O_3 grains. This model is consistent with the TEM and ED results discussed above, as well as with the data available in the literature [23,73]. As a result of the adsorption of CH_4 molecules and the activation of oxygen along the perimeter of the In_2O_3/Au contact, a decrease in the Schottky potential barriers occurs at the grain boundary. Thus, when gold ions are introduced into indium hydroxide sol, followed by joint formation of the In_2O_3–Au^{III} system, the decisive role in determining the sensitivity belongs to the intergranular contacts and current transfer in them.

The sensitivity of In_2O_3–Au,*Cit* sensors to CH_4 at high temperature (the second maximum) was found to be low, which might be due to the high electrical conductivity of the sensors. The effect of low response of indium oxide sensors at elevated temperature is consistent with the idea that the current at high temperature may be controlled by the so-called "non-surface type" current transport. This type is different from the surface type, which is characteristic of, for example, SnO_2 [18,28,74]. It has been shown how the properties of sensors can be changed by controlling this type of conductivity [74]. In the process of the sol–gel synthesis, indium oxide grains presumably form conductivity channels characterized by the absence of energy barriers in them [47,51]. Whereas In_2O_3–Au^{III} is the only material where Schottky energy barriers are created at the grain boundaries, which might be due to the location of gold atoms on the lateral faces of indium oxide.

4. Conclusion

The aim of the research was to prepare In_2O_3–Au nanomaterials with AuNPs smaller than 5 nm and to study their properties as sensing elements for reducing gases. Samples of In_2O_3–Au with AuNP diameters of 1.5 and 3.5 nm have been prepared. Within this range of AuNPs sizes, the quantum-size effect is most pronounced, which can significantly change the electronic and, as a consequence, the adsorption-catalytic properties of gold in comparison with its bulk state. However, in order to obtain AuNPs with the mentioned sizes, we had to reduce significantly the gold concentration relative to the one optimal for In_2O_3–Au gas sensor operation.

Due to the low gold concentration, the measurement techniques used to characterize the structure of In_2O_3 phase and AuNPs (TEM, XPS, EPR) turned out to be insufficiently effective. They did not allow revealing certain subtle differences in the surface properties of gold particles and indium oxide, which are essential for effective detection and justification of the mechanism of this process. At such low gold concentration, the density of gold particles per unit volume is low. Therefore, any significant changes in the sensor parameters were not expected.

However, in spite of the low concentration, AuNPs with d = 1.5–3 nm were found to have a significant effect on both electrical resistance and sensitivity of indium oxide when detecting CO, acetone, and methane. A correlation between the Au particle size and the response of In_2O_3–Au sensors to CO and acetone was revealed. Gold particles with a diameter of 3.5 nm are more active compared to those with d_{Au} = 1.5 nm. The sensitivity of all the studied sensors to methane in the region of maximum electrical resistance at 360 °C is nearly identical and does not depend on either Au grain size or the method of its introduction into In_2O_3.

However, at 400–450 °C (high-temperature maximum), a significant increase in the response of In_2O_3–Au sensors to methane is achieved by the introduction of gold in ionic form rather than as nano-sized metal particles. This phenomenon is explained by a significant increase in the electrical resistance of indium oxide due to the creation of energy barriers (Schottky barriers) at the interface of In_2O_3 grains.

The obtained results support for the difficulty of establishing a clear correlation between the AuNPs size and the parameters of In_2O_3–Au sensors to methane, CO, and acetone. The fact that the samples were prepared using different gold introduction techniques and applying stabilizers of various chemical nature, complicates the revealing of correlations between the AuNPs size and In_2O_3–Au sensitivity. There is no single technology for introducing AuNPs with a particle size adjustable over a wide range and their uniform high-density distribution on oxide materials yet. The development of such a technology is highly desirable for creating efficient Au/metal oxide sensors.

To achieve a significant effect of gold on the properties of In_2O_3 sensors, a higher AuNPs density (than in the studied samples) in the bulk or on the oxide surface is required. For sensors with polycrystalline sensing layers, it is important that nano-sized gold particles are located near the contacts between metal oxide grains. An introduction of highly concentrated colloidal solutions of gold with adjustable AuNPs size might become a promising approach to achieve this goal. However, an effective stabilizer for gold particles is required in this case. The search for such stabilizers or their synthesis can solve the problem of introducing AuNPs of uniform size with a high density of their distribution per unit area or volume of oxide. This would make it possible to create sensors based on "Au/metal oxide" materials, which are promising for various applications. In particular, they are of interest for the selective detection of low concentrations of CO, as well as some organic substances. Besides, the In_2O_3–Au system might serve as a model for studying the adsorption-catalytic properties of nano-sized gold for the case of strong "metal/oxide" interaction.

CRediT authorship contribution statement

M. Ivanovskaya: Conceptualization, Writing – original draft. **E. Ovodok:** Investigation, Writing – review & editing. **D. Kotsikau:** Formal analysis, Investigation, Writing – review & editing. **I. Azarko:** Formal analysis, Investigation. **M. Micusik:** Formal analysis, Investigation.

Declaration of competing interest

The authors declare that they have no known competing financial

interests or personal relationships that could have appeared to influence the work reported in this paper.

Acknowledgment

The work was carried out within the framework of research work 2.1.04.02 SPNI "Chemical Processes, Reagents and Technologies, Bio-regulators and Bioorganic Chemistry".

The authors express their gratitude to V. Kormosh for measuring the characteristics of the sensors, which was carried out under the project Belarusian-Ukrainian project (grant no. 0121U14006, Ukraine).

Data availability

Data will be made available on request.

References

[1] M. Haruta, Gold as a novel catalyst in the 21st century: Preparation, working mechanism, and applications, Gold Bull. 37 (2004) 27–36, https://doi.org/10.1007/BF03215514.
[2] Nanoparticles: Building blocks for nanotechnology. Edited by Vincent Rotello. NewYork Boston 2004. 284 p.
[3] M.-C. Daniel, D. Astruc, Gold Nanoparticles: Assembly, Supramolecular Chemistry, Quantum-Site-Related Properties, and Applications toward Biology, Catalysis, and Nanotechnology, Chem. Rev. 104 (2004) 293–345, https://doi.org/10.1021/cr030698+.
[4] J. Li, S. Zhang, Y. Zheng, N. Luo, B. Zhang, Y. Wang, Enhanced CO sensor based on In_2O_3 nanocubes with decoration of Au under high humidity: Experimental combined with theoretical study, Microchem. J. 201 (2024) (2024) 110614, https://doi.org/10.1016/j.microc.2024.110614.
[5] Y. Zhang, X. Yang, X. Yan, Z. Sun, Z. Hu, W. Liu, Y. Cheng, G. Pan, Au-sensitized metal–organic framework-derived indium-doped zinc oxide for highly enhanced trimethylamine sensing, Microchem. J. 207 (2024) 111838, https://doi.org/10.1016/j.microc.2024.111838.
[6] F. Cosandey, T.E. Madey, Growth, morphology, interfacial effects and catalytic properties of Au on TiO_2, Surf. Rev. Lett. 08 (01n04) (2001) 73–93, https://doi.org/10.1142/S0218625X01000884.
[7] S.A. Carabineiro, N. Bogdanchikova, M. Avalos-Borja, A. Pestryakov, P.B. Tavares, J.L. Figueiredo, Gold supported on metal oxides for carbon monoxide oxidation, Nano Res. 4 (2011) 180–193, https://doi.org/10.1007/s12274-010-0068-7.
[8] S.A.C. Carabineiro, A.M.T. Silva, G. Dražić, P.B. Tavares, J.L. Figueiredo, Gold nanoparticles on ceria supports for the oxidation of carbon monoxide, Catal. Today 154 (2010) 21–30, https://doi.org/10.1016/j.cattod.2010.01.036.
[9] A.C. Gluhoi, N. Bogdanchikova, B.E. Nieuwenhuys, The effect of different types of additives on the catalytic activity of Au/Al_2O_3 in propene total oxidation: transition metal oxides and ceria, J. Catal. 229 (2005) 154–162, https://doi.org/10.1016/j.jcat.2004.10.003.
[10] M. Haruta, S. Tsubota, T. Kobayashi, H. Kageyama, M.J. Genet, B. Delmon, Low-Temperature Oxidation of CO over Gold Supported on TiO_2, α-Fe_2O_3, and Co_3O_4, J. Catal. 144 (1993) 175–192, https://doi.org/10.1006/jcat.1993.1322.
[11] Y. Iizuka, T. Tode, T. Takao, T. Ken-ichiro Yatsu, S. Takeuchi, M.H. Tsubota, A Kinetic and Adsorption Study of CO Oxidation over Unsupported Fine Gold Powder and over Gold Supported on Titanium Dioxide, J. Catal. 187 (1999) 50–58, https://doi.org/10.1006/jcat.1999.2604.
[12] T. Tsukuda, Toward an Atomic-Level Understanding of Size-Specific Properties of Protected and Stabilized Gold Clusters, Bull. Chem. Soc. Jpn 85 (2012) 151–168, https://doi.org/10.1246/bcsj.20110227.
[13] M. Haruta, Size- and support-dependency in the catalysis of gold, Catal. Today 36 (1997) 153–166, https://doi.org/10.1016/S0920-5861(96)00208-8.
[14] M. Haruta, M. Daté, Advances in the catalysis of Au nanoparticles, Appl. Catal. A: General 222 (2001) 427–437, https://doi.org/10.1016/S0926-860X(01)00847-X.
[15] T. Akita, S. Tanaka, K. Tanaka, M. Haruta, M. Kohyama, Sequential HAADF-STEM observation of structural changes in Au nanoparticles supported on CeO_2, J. Mater. Sci. 46 (2011) 4384–4391, https://doi.org/10.1007/s10853-011-5370-6.
[16] X. Lin, N. Nilius, M. Sterrer, P. Koskinen, H. Häkkinen, H.J. Freund, Characterizing low-coordinated atoms at the periphery of MgO-supported Au islands using scanning tunneling microscopy and electronic structure calculations, Phys. Rev. B. 81 (2010) 153406, https://doi.org/10.1103/PhysRevB.81.153406.
[17] I.X. Green, W. Tang, M. Neurock, J.T. Yates Jr, Spectroscopic Observation of Dual Catalytic Sites During Oxidation of CO on a Au/TiO_2 Catalyst, Science 333 (2011) 736–739, https://doi.org/10.1126/science.1207272.
[18] M. Okumura, S. Tsubota, M. Haruta, Preparation of supported gold catalysts by gas-phase grafting of gold acethylacetonate for low-temperature oxidation of CO and of H_2, J. Mol. Catal. A: Chem. 199 (2003) 73–84, https://doi.org/10.1016/S1381-1169(03)00020-7.
[19] Q. Fu, T. Wagner, Interaction of nanostructured metal overlayers with oxide surfaces, Surf. Sci. Rep. 62 (2007) 431–498, https://doi.org/10.1016/j.surfrep.2007.07.001.
[20] F. Boccuui, S. Tsubota, M. Haruta, Vibrational investigation of CO adsorbed on gold deposited on TiO_2, J. Electron Spectroscopy Related Phenomena 64 (1993) 241–250, https://doi.org/10.1016/0368-2048(93)80085-Z.
[21] M. Haruta, M. Daté, Advances in the catalysis of Au nanoparticles, Appl. Catal. A 222 (2001) 427–437, https://doi.org/10.1016/S0926-860X(01)00847-X.
[22] D. Degler, S.A. Müller, D.E. Doronkin, D. Wang, J.D. Grunwaldt, U. Weimar, N. Barsan, Platinum loaded tin dioxide: a model system for unravelling the interplay between heterogeneous catalysis and gas sensing, J. Mater. Chem. A 6 (2018) 2034–2046, https://doi.org/10.1039/C7TA08781K.
[23] S. Basu, P.K. Basu, Nanocrystalline Metal Oxides for Methane Sensors: The Role of Noble Metals, J. Sens. 1 (2009) 861968, https://doi.org/10.1155/2009/861968.
[24] M. Masikini, M. Chowdhury, O. Nemraoui, Review—Metal Oxides: Application in Exhaled Breath Acetone Chemiresistive Sensors, J. Electrochem. Soc. 167 (2020) 037537, https://doi.org/10.1149/1945-7111/ab64bc.
[25] A.A. Abokifa, K. Haddad, J. Fortner, C.S. Lo, P. Biswas, Sensing mechanism of ethanol and acetone at room temperature by SnO_2 nano-columns synthesized by aerosol routes: theoretical calculations compared to experimental results, J. Mater. Chem. A 6 (2018) 2053–2066, https://doi.org/10.1039/C7TA09535J.
[26] K.L. Morulane, H.C. Swart, D.E. Motaung, A review on topical advancement and challenges of indium oxide based gas sensors: Future outlooks, J. Environ. Chem. Eng. 12 (2024) 112144, https://doi.org/10.1016/j.jece.2024.112144.
[27] J. Hwang, H. Jung, H.S. Shin, D.S. Kim, B.K. Ju, M. Chun, The effect of noble metals on CO gas sensing properties of In_2O_3 nanopartilcles, Appl. Sci. 11 (2021) 4903, https://doi.org/10.3390/app11114903.
[28] D. Degler, U. Weimar, N. Barsan, Current Understanding of the Fundamental Mechanisms of Doped and Loaded Semiconducting Metal-Oxide-Based Gas Sensing Materials, ACS Sens. 4 (2019) 2228–2249, https://doi.org/10.1021/acssensors.9b00975.
[29] D. Degler, S. Rank, S. Mueller, H.W.P. de Carvalho, J.-D. Grunwaldt, U. Weimar, N. Barsan, Gold-Loaded Tin Dioxide Gas Sensing Materials: Mechanistic Insights and the Role of Gold Dispersion, ACS Sens 1 (2016) 1322–1329, https://doi.org/10.1021/acssensors.6b00477.
[30] G. Korotcenkov, V. Brinzari, B.K. Cho, Conductometric gas sensors based on metal oxides modified with gold nanoparticles: a review, Microchim. Acta 183 (2016) 1033–1054, https://doi.org/10.1007/s00604-015-1741-z.
[31] M. Ivanovskaya, E. Ovodok, T. Gaevskaya, D. Kotsikau, V. Kormosh, V. Bilanych, M. Micusik, Effect of Au nanoparticles on the gas sensitivity of nanosized SnO_2, Mater. Chem. Phys. 258 (2021) 123858, https://doi.org/10.1016/j.matchemphys.2020.123858.
[32] E. Ovodok, V. Kormosh, V. Bilanych, M. Ivanovskaya, Semiconductor Metal Oxides Doped with Gold Nanoparticles for Use in Acetone Gas Sensors, J. Phys.: Conf. Ser. 2315 (2022) 012018. DOI 10.1088/1742-6596/2315/1/012018.
[33] G. Korotcenkov, V. Brinzari, S.H. Han, B.K. Cho, Gas-sensing properties of In_2O_3 films modified with gold nanoparticles, Mater. Chem. Phys. 175 (2016) 188–199, https://doi.org/10.1016/j.matchemphys.2016.03.018.
[34] M.I. Ivanovskaya, E.A. Ovodok, D.A. Kotikau, Gas-sensitivity properties of nanoscale Au-In_2O_3 materials, Russ. J. Gen. Chem. 81 (2011) 2074, https://doi.org/10.1134/S1070363211100069.
[35] M.I. Ivanovskaya, E.A. Ovodok, D.A. Kotsikau, Interaction of carbon monoxide with In_2O_3 and In_2O_3-Au nanocomposite, J. Applied Spectroscopy 78 (2012) 842–847, https://doi.org/10.1007/s10812-012-9542-1.
[36] N. Izu, T. Itoh, M. Nishibori, W. Shin, Effects of noble metal addition on response of ceria thick film CO sensors, Sens. Actuators B 171–172 (2012) 350–353, https://doi.org/10.1016/j.snb.2012.04.058.
[37] J.H.W. De Wit, Structural Aspects and Defect Chemistry in In_2O_3, J. Solid State Chem. 20 (1977) 143–148, https://doi.org/10.1016/0022-4596(77)90061-5.
[38] G.N. Gerasimov, V.F. Gromov, M.I. Ikim, O.J. Ilegbusi, L.I. Trakhtenberg, Effect of interaction between components of In_2O_3-CeO_2 and SnO_2-CeO_2 nanocomposites on structure and sensing properties, Sens. Actuators b: Chem. 279 (2019) 22–30, https://doi.org/10.1016/j.snb.2018.09.093.
[39] W. Liu, L. Xu, K. Sheng, X. Zhou, B. Dong, G. Lu, H. Song, A highly sensitive and moisture-resistant gas sensor for diabetes diagnosis with Pt@In_2O_3 nanowires and a molecular sieve for protection, NPG Asia Mater. 10 (2018) 293–308, https://doi.org/10.1038/s41427-018-0029-2.
[40] R. Xing, Q. Li, L. Xia, J. Song, L. Xu, J. Zhang, Y. Xie, H. Song, Au-modified three-dimensional In_2O_3 inverse opals: synthesis and improved performance for acetone sensing toward diagnosis of diabetes, Nanoscale 7 (2015) 13051–13060, https://doi.org/10.1039/C5NR02709H.
[41] Q. Xie, Y. Ding, Q. Wang, P. Song, Fabrication of 1D/2D In2O3 Nanofiber/Ti3C2TX MXene Composites for High-Efficiency Trimethylamine Detection at Low Temperature, Sensors Actuators 405 (2024) 35338, https://doi.org/10.1016/j.snb.2024.135338.
[42] S. Zhang, Y. Ding, Q. Wang, P. Song, MOF-Based Ternary Nanocomposites In_2O_3/ZnO/$Ti_3C_2T_X$ MXene for Determination of Ethanol Content at Room Temperature, Sensors Actuators 393 (2023) 134122, https://doi.org/10.1016/j.snb.2023.134122.
[43] S. Americo, E. Pargoletti, R. Soave, F. Cargnoni, M.I. Trioni, G.L. Chiarello, G. Cerrato, G. Cappelletti, Unveiling the acetone sensing mechanism by WO_3 chemiresistors through a joint theory-experiment approach, Electrochim. Acta 371 (2021) 137611, https://doi.org/10.1016/j.electacta.2020.137611.
[44] A. Tricoli, M. Righettoni, A. Teleki, Semiconductor Gas Sensors: Dry Synthesis and Application, Angew. Chem. Int. Ed. 49 (2010) 7632–7659, https://doi.org/10.1002/anie.200903801.
[45] F. Boccuzzi, A. Chiorino, S. Tsubota, M. Haruta, An IR study of CO sensing mechanism on Au/ZnO, Sens. Actuators B 24–25 (1995) 540–543, https://doi.org/10.1016/0925-4005(95)85117-8.

[46] A.-K. Elger, C. Hess, Elucidating the Mechanism of Working SnO_2 Gas Sensors Using Combined Operando UV/Vis, Raman, and IR Spectroscopy, Angew. Chem. Int. Ed. 58 (2019) 15057–15061, https://doi.org/10.1002/anie.201908871.
[47] M.I. Ivanovskaya, E.A. Ovodok, D.A. Kotsikau, Sol-gel synthesis and features of the structure of Au-In_2O_3 nanocomposites, Glas. Phys. Chem. 37 (2011) 560, https://doi.org/10.1134/S1087659611050051.
[48] S.V. Voitekhovich, A. Wolf, C. Guhrenz, et al., 5-(2-Mercaptoethyl)-1H-tetrazole: Facile Synthesis and Application for the Preparation of Water Soluble Nanocrystals and Their Gels, Chem. Eur. J. 22 (2016) 14746–14752, https://doi.org/10.1002/chem.201602980.
[49] C. Guhrenza, A. Wolfa, M. Adam, L. Sonntag, S.V. Voitekhovich, S. Kaskel, N. Gaponik, A. Eychmuller, Tetrazole-Stabilized Gold Nanoparticles for Catalytic Applications, Z. Phys. Chem. 231 (2017) 51–62, https://doi.org/10.1515/zpch-2016-0879.
[50] R. Javakantha, K.A.A. Gamage, N. Bandara, M. Karunarathne, M. Seneviratne, E. Comini, D. Zappa, N. Gunawardhana, Fabrication of Automated Hydrostatic Pressure-Based Densitometer with a Calibrated Pressure Sensor, Sci 6 (2024) 41, https://doi.org/10.3390/sci6030041.
[51] M. Ivanovskaya, Ceramic and film metaloxide sensors obtained by sol-gel method: structural features and gas-sensitive properties, Electron Technology 33 (2000) 108–112.
[52] Y. Li, L. Qiao, D. Yan, L. Wang, Y. Zeng, H. Yang, Preparation of Au-sensitized 3D hollow SnO_2 microspheres with an enhanced sensing performance, J. Alloy. Compd. 586 (2014) 399–403, https://doi.org/10.1016/j.jallcom.2013.09.147.
[53] W. Haiss, N.T.K. Thanh, J. Aveyard, D.G. Fernig, Determination of Size and Concentration of Gold Nanoparticles from UV-Vis Spectra, Anal. Chem. 79 (2007) 4215–4221, https://doi.org/10.1021/ac0702084.
[54] F. Berger, E. Beche, R. Berjoan, D. Klein, A. Chambaudet, An XPS and FTIR study of SO_2 adsorption on SnO_2 surfaces, Appl. Surf. Sci. 93 (1996) 9–16, https://doi.org/10.1016/0169-4332(95)00319-3.
[55] K. Yura, K.C. Fredrikson, E. Matijevic, Preparation and Properties of Uniform Colloidal Indium Compounds of Different Morphologies, Colloids Surf. 50 (1990) 281–293, https://doi.org/10.1016/0166-6622(90)80270-E.
[56] J.R. Bolton, J.E. Wertz, Electron spin resonance: elementary theory and practical applications, second ed., Wiley-Interscience, 2008.
[57] M. Ivanovskaya, P. Bogdanov, Effect of Ni^{II} Ions on the Properties of In_2O_3-based Ceramic Sensors, Sens. Actuators B 53 (1998) 44–53, https://doi.org/10.1016/S0925-4005(98)00281-0.
[58] E.V. Frolova, M.I. Ivanovskaya, Structural Defects Formation in the Inorganic Sol-Gel derived Oxides, Defect and Diffusion Forum, Trans Tech Publications Ltd, Switzerland, 242-244 (2005) 143-158. https://doi.org/10.4028/www.scientific.net/DDF.242-244.143.
[59] A.K. Kolosov, V.A. Shvets, V.B. Kazansky, ESR of O^- and O^{2-} stabilized on ^{95}Mo ions in a molybdenum-silica gel support system, Chem. Phys. Let. 34 (1975) 360–362, https://doi.org/10.1016/0009-2614(75)85293-6.
[60] O.F. Schirmer, Trapped-hole centers containing lithium in MgO, CaO and SrO, J. Phys. Chem. Solid 32 (1971) 499–509, https://doi.org/10.1016/0022-3697(71)90034-5.
[61] M. Che, A.J. Tench, Characterization and Reactivity of Mononuclear Oxygen Species on Oxide Surfaces, Adv. Catalysis 31 (1982) 78–133, https://doi.org/10.1016/S0360-0564(08)60453-8.
[62] V.P. Popov, L.V. Morozova, Electric conductivity and thermodynamics of indium oxide and indium oxide based solid solutions reduction process, Russ. J. Inorg. Chem. 40 (1995) 37–41.
[63] K. Sasaki, H.P. Seifert, L.J. Gauckler, Electronic conductivity of In_2O_3 solid solution with ZrO_2, J. Electrochem. Soc. 141 (1997) 2759–2768, https://doi.org/10.1149/1.2059204.
[64] J.E. Nicholls, J.J. Davies, An optically-detected magnetic resonance investigation of recombination emission in indium doped zinc sulphide, J. Phys. C: Solid St. Phys. 13 (1980) 2393–2405, https://doi.org/10.1088/0022-3719/13/12/019.
[65] M. Okumura, J.M. Coronado, J. Soria, M. Haruta, EPR study of CO and O_2 interaction with supported Au catalysts, J. Catal. 203 (2001) 168–174, https://doi.org/10.1006/jcat.2001.3307.
[66] D. Briggs, M.P. Seah, Practical Surface Analysis by Auger and X-ray Photoelectron Spectroscopy, John Wiley and Sons Ltd., Chichester, 1983.
[67] A.W.C. Lin, N.R. Armstrong, T. Kuwana, X-ray photoelectron/auger electron spectroscopic studies of tin and indium metal foils and oxides, Anal. Chem. 49 (1977) 1228–1235, https://doi.org/10.1021/ac50016a042.
[68] N. Kruse, S. Chenakin, XPS characterization of Au/TiO_2 catalysts: Binding energy assessment and irradiation effects, Appl. Catal. A 391 (2011) 367–376, https://doi.org/10.1016/j.apcata.2010.05.039.
[69] M. Ivanovskaya, P. Bogdanov, G. Faglia, G. Sberveglieri, The Features of Thin Film and Ceramic Sensors for the Detection of CO and NO_2, Sens. Actuators B 68 (2000) 344–350, https://doi.org/10.1016/S0925-4005(00)00455-X.
[70] T. Kimakova, D. Kondrakhova, E. Ovodok, M. Ivanovskaya, B. Kormosh, S. Vorobiov, M. Lisnichuk, V. Bilanych, V. Komanicky, Sensors Based on Tin and Indium Oxides for the Determination of Acetone in Human Breath, ACS Omega 8 (2023) 4007840086, https://doi.org/10.1021/acsomega.3c02 125.
[71] V.F. Kiselev, O.V. Krylov, Adsorption and Catalysis on Oxides of Transition Metals. Adsorption and Catalysis on Transition Metals and Their Oxides, Springer, Berlin, Heidelberg, 1989, pp. 136–265.
[72] D. Kohl, Surface Processes in the Detection of Reducing Gases with SnO_2-Based Devices, Sens. Actuators B 18 (1989) 71–113, https://doi.org/10.1016/0250-6874(89)87026-X.
[73] Y. Maeda, M. Okumura, S. Tsubota, M. Kohyama, M. Haruta, Local barrier height of Au nanoparticles on a TiO_2 (110)-(1×2) surface, Appl. Surf. Sci. 222 (2004) 409–414, https://doi.org/10.1016/j.apsusc.2003.09.007.
[74] N. Murayama, Nanostructural design of electrically conductive ceramics and its application in gas sensors, J. Ceram. Soc. Japan 116 (2008) 1167–1174, https://doi.org/10.2109/jcersj2.116.1167.